Archives of Materials Science and Engineering

Volume 98
Issue 1
July 2019
Pages 5-31

International Scientific Journal
published monthly by the
World Academy of Materials
and Manufacturing Engineering

DOI: 10.5604/01.3001.0013.3391

Copper infiltrated high speed steel skeletons

M. Madej
Faculty of Metal Engineering and Industrial Computer Science, AGH University of Science and Technology, Al. Mickiewicza 30, 30-059 Kraków, Poland
Corresponding e-mail address: mmadej@agh.edu.pl

ABSTRACT

Purpose: This article is a monographic summary of the most important research results from the last 10 years regarding HSS based materials. This materias were produced with powder metallurgy technology using spontaneous infiltration. The presented results answer the question of how iron, tungsten carbide and copper additives influence the final properties of these materials and present additional microstructural phenomena revealed during their manufacture.

Design/methodology/approach: Materials were produced by spontaneous infiltration. Porous skeletons for infiltration were produced by pressing and pressing and sintering of mixed powders. Copper was used as the infiltrant.

Findings: The molten copper was drawn into the porous skeletons, through a capillary action, and filled virtually the entire pore volume to get the final densities exceeding 97% of the theoretical value.

Research limitations/implications: As part of further research, microstructures of M30WC composites obtained by direct infiltration of copper into as-sintered porous skeletons using TEM are planned.

Practical implications: Efficiant mechanical strength, high hardness, adequate heat resistance and good wear resistance of M3 type 2 HSS powder produced by woter atomisation make it an attractive material for manufacture of valve train components, for example valve seat inserts.

Originality/value: The novelty in the article are the results of research on the microstructure made using TEM, the results of testing materials after heat treatment, untypical for high-speed steels. The article attempts to explain the influence of iron addition on properties - such a slight loss of mass as a result of its addition. The second aim of this work is to analyse the microstructural changes during sintering porous skeletons made from HSS with WC additions.

Keywords: High speed steels, Iron, Tungsten carbide, Powder metallurgy, Infiltration, Sintering, Microstructure

Reference to this paper should be given in the following way:

M. Madej, Copper infiltrated high speed steel skeletons, Archives of Materials Science and Engineering 98/1 (2019) 5-31.

MATERIALS

1. Introduction

High speed steels consist of a family of alloy elements used most often for the production of cutting tools. The name of this type of steel – high speed steel – is a combination of the following features [1,2]:

a) the alloys belong to the steels with high content of carbon and –X multicomponent system, where X represents a group of alloying elements in which Cr, W or Mo, V, Co and sometimes Ni are the principal ones;
b) the alloys are characterized by their maintence to retain fficiant hardness, when exposed to an elevated temperatures arising from cutting at high speeds different materials. HSS are produced by powder metallurgy and by the classic metallurgical methods [2-4].

Some applications of tool steels produced by powder technology are in conditions where the priority is good wear resistance. Examples include cam followers, valve seat inserts, and oil pump components. In this application, the material must exhibit also resistance to oxidation, high hot strength and hardness. Typical cold compaction single or double-sided and sintering in vacuum atmosphere of PM high speed steels (HSSs) to full density is now well-known technique [5-14]. A good solution in relation to the presented requirements may be achieved by using mixtures of high speed steel powders with low alloy powders or pure iron powder, for axemple Hoganas NC100.24. During sintering or sintering and infiltration of such the mixtures, interdiffusion of both carbon and metallic alloying elements from HSSs matrix occurs. In the particular case of copper infiltrated iron and steel compacts, the base iron matrix, or porous skeleton, is heated in contact with the copper alloy to a temperature exceeding the melting point of copper, normally to between 1100 and 1150°C. Materials of this type can be produced using the basic techniques of powder metallurgy: infiltration technique. Because of technological and economic considerations are just as important, infiltration of a high steel based porous skeleton with liquid copper has proven to be a good technique by which fully dense material is produced at low cost [5,6,10,11]. Infiltration is an operation in which the pores of the PM part are filled with a molten metal using capillary forces [15] or external pressure – pressure infiltration [16]. The melting point of the filler metal must be below that of the PM part and during heating the filler metal in contact with the sintered component, so capillary action draws the filler into the capillaries of porous skeleton. The microstructure after infiltration process is relatively nonporous, and the infiltrated part has a more uniform density, as well as improved toughness and strength. Infiltration by liquid infiltrant can be made by in many ways, it can be pressureless infiltration, vacuum pressure infiltration, squeeze casting, compocasting, etc.

Another part of work has been undertaken to sinter metal matrix composites which contain ceramic particles embedded in a HSSs matrix. Most studies have been focused on sintered HSSs with additions of deifferent carbides or oxides such as Al_2O_3, VC, NbC, TiC, WC and TiN with the aim of producing a HSSs based composites with good wear resistant [17-29]. These composites have been developed for difficult wear conditions as an attractive alternative to expensive sintered metal and ceramic tool materials based on cobalt, which are now replaced element in any materias. They have higher hardness, good elastic modulus and resistance to wear than high strength steels, however, the addition of brittle ceramic particles may cause degradation of toughness as the reinforcing particles could cause crack initiation and than its propagations. To ensure a good connection between the ceramic/matrix, the ceramic particles must show little reactivity with the matrix in which they are located with exception for Al_2O_3, which does not react with most of the materials to which it is added. Diffusion of pure iron, in which the high speed steel matrix is rich, to MC type carbide particles give rise to good cohesion across the ceramic/matrix interface. Besides, MC type carbides are relatively stable in contact with iron during sintering and do not dissolve extensively so this is why the MC type particles were mainly chosen as the reinforcement in this composites. An easy technologically and almost cheap route to develop high speed steels reinforced with MC carbides consists of mixing any commercial high speed steel powders with any carbide MC type powder available on the market and stable in contact with steel. Good mechanical properties and its heat resistance and efficient wear resistance of high speed steels make them an attractive material for manufacture MMC.

Presentation of the results and their analysis will be divided into two parts, one will concentrate on HSS – iron materials and the other on high speed steel based composites with addition of WC.

2. Experimental procedure

Water atomised M3 type 2 powder, finer than 160 μm, was delivered by POWDREX SA in as-annealed condition. It's microstructure consists of fine carbides embedded in a artensitic/bainitic matrix. Typical particle microhardness HV0.065 is of 284 ± 17 [29,30]. The chemical composition of the M3/2 grade powder is given in Table 1.

The following compositions were investigated:

1. M3/2 **M**
2. M3/2 + 20 wt % Fe **M20Fe**
3. M3/2 + 50 wt % Fe **M50Fe**
4. M3/2 + 10 wt% WC **M10WC**
5. M3/2 + 30 wt% WC **M30WC**

The morphology of powders used for research is shown in the Figures 1-4.

Table 1.
The chemical composition of the experimental M3 type 2 powder, wt.%

C	Cr	Co	Mn	Mo	Ni	V	W	Fe	O
1.23	4.27	0.39	0.21	5.12	0.32	3.1	6.22	balance	0.0626

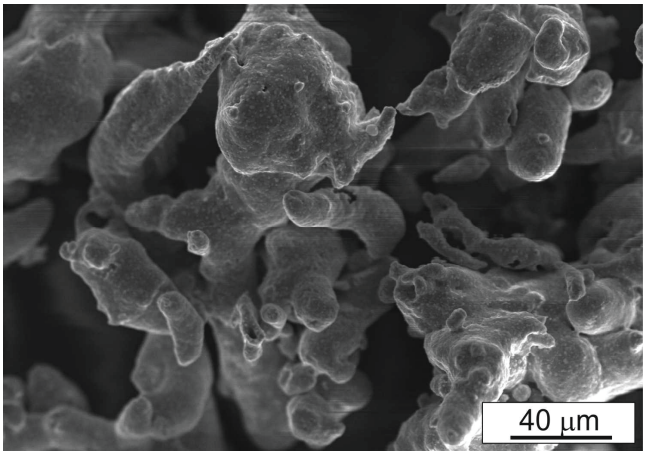

Fig. 1. The morphology of M3/2 powders, SEM

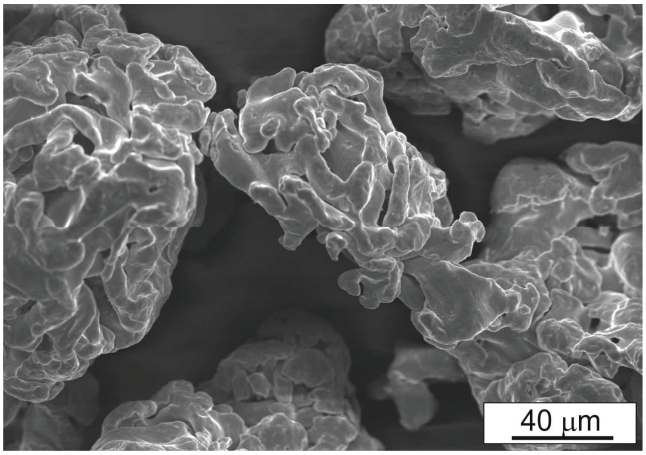

Fig. 2. The morphology of Fe NC100.24 powders, SEM

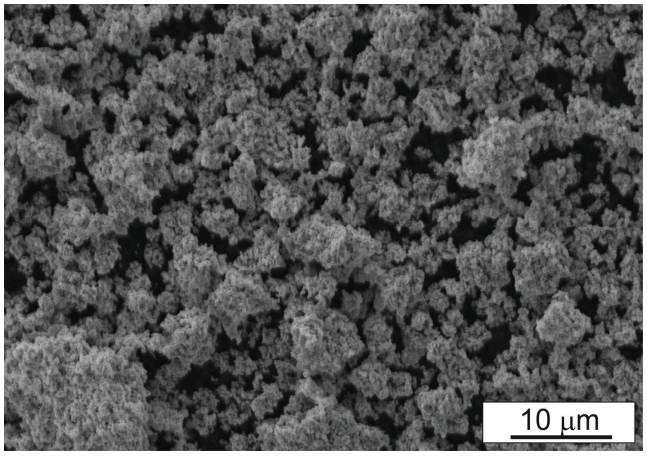

Fig. 3. The morphology of tungsten carbide WC powders, SEM

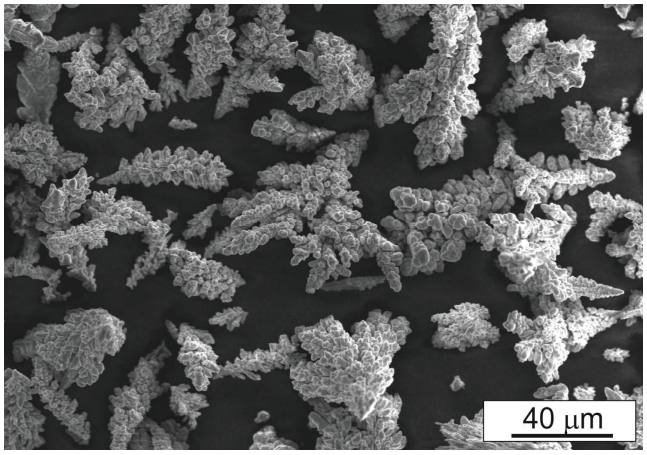

Fig. 4. The morphology of copper ECu.1 powders, SEM

The powders mixtures were prepared by mixing its for 30 minutes in a Turbula® T2F mixer. Powder mixtures were cold pressed in a rigid cylindrical die at 800 MPa without the use of lubricants. There were two types of porous skeletons used for infiltration: green compacts and as-skeletons were measured prior to infiltration using the Archimedes method (MPIF standard no 42). The theoretical densities for the composites were calculated using the following formula (1):

$$\rho t = (\rho a \cdot Xa + \rho b \cdot Xb) \quad (1)$$

where:

ρa – density of Fe or WC additions;
Xa – volume fraction of Fe or WC additions;
ρb – density of M3 type 2 HSS;
Xb – volume fraction of M3 type 2 HSS.

The measured densities were divided by theoretical densities (ρ_t) to calculate relative densities.

The infiltration process was carried out in vacuum better than 10^{-2} Pa. Porous skeletons (green compacts and preforms sintered for 60 minutes at 1150°C in vacuum) were infiltrated with copper. Carefully pre-weighed green compacts of copper infiltrant were placed on top of the porous skeletons of predetermined porosity, heated to 900°C with isothermal stops for 30 minutes and then heated to 1150°C, held at temperature for 15 minutes, and cooled down with the furnace to room temperature.

The infiltrated specimens were subsequently tested for brinell hardness, three point bending strength, wear resistance, and subjected to microstructural examinations by means of both scanning electron microscopy (SEM) and transmission electron microscopy (TEM). The tribological tests were carried out using the block-on-ring tester produced by ITEE Radom (Fig. 5).

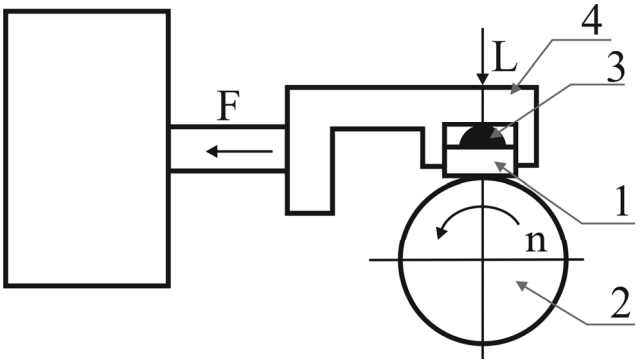

Fig. 5. Wear test principle on Tribosystem T05

During the test, a rectangular test for wear (1) is mounted in a dedicated holder (4) equipped with a rounded insert (3) ensuring a constant linear and surface contact between the sample and the counter-sample being a steel ring (2) rotating at a given speed. The surface of the sample wear is set perpendicular to the direction in which the load is exerted. The device has a double lever system to load the sample towards the ring with a load accuracy of 1%.

The wear test conditions were:

- test dimension of the sample was: 20 x 4 x 4 mm,
- rotating ring: heat treated steel 100Cr6, 55 HRC, ø49.5 x 8 mm,
- rotational speed: 500 r/min ±1,
- load: 165 N,
- sliding distance, continous from start to stop: 1000 m.

The parameters measured during the test were:

- loss of sample mass (Δm),
- friction force F (used to calculate the coefficient of friction).

3. Results

3.1. Porous skeletons

The first step of the production process was to prepare the porous skeletons for infiltration process. There were two ways to produce its: pressing and compacting and sintering.

A fully-dense material made of the M3 type 2 powder can be achieved by sintering at around 1250°C with sintering window ±5° [7,27], therefore to produce porous preforms the compacts were sintered at 1150°C for one hour. The combined effects of the powder mix composition and its processing route on relative densities of the porous skeletons are shown in Figure 6.

The addition of iron causes a slight increase in density. and the scale of increasing depends on the iron content in the powder mixture. From Figure 6 it is also evident that the as-sintered densities of M and M50Fe are approximately equal to their green densities. Figure 6 also show, the effect of WC additions on compressibility and shrinkage of the M HSS powder. It is obvious that the green density of compact decreases with increasing of tungsten carbide content. This attributes to hard and non-deforming nature of the tungsten carbide WC reinforcements, which constricts HSS-particle deformation,

sliding and rearrangement during compaction. Compacting of HSS-WC mixtures are also inhibited by the presence of agglomerates of tungsten carbide powder that failed to be crushed while mixing in a Turbula mixer. Additions of 30% tungsten carbide increase the as-sintered density probably due to presence of an intermediate liquid phase, resulting from presence of free carbon which are from the dissolving of tungsten carbide particles. In order to identify the phenomena occurring during sintering, this process was also studied by means of dilatometric measurements.

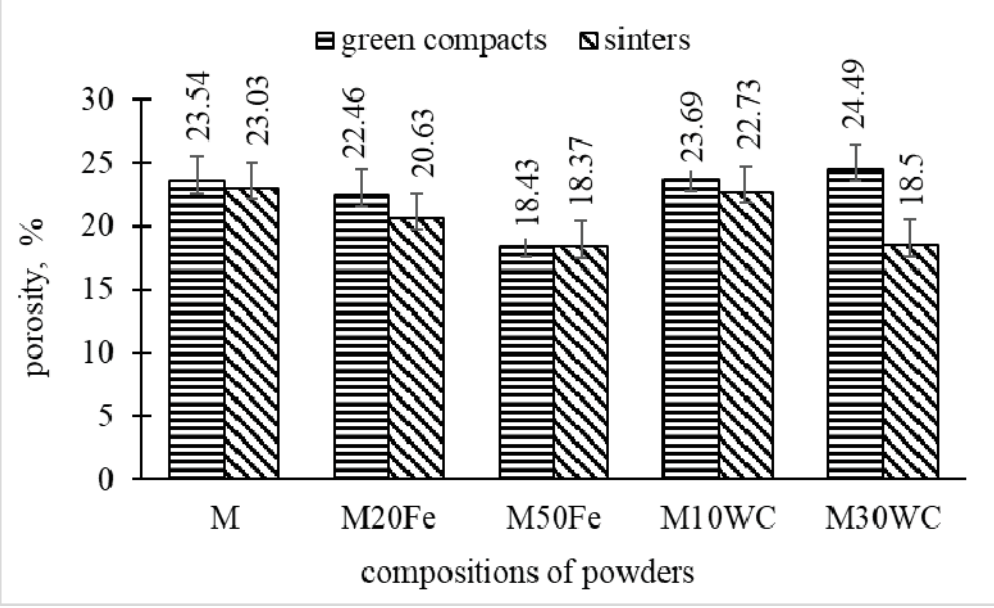

Fig. 6. The porosity level of green compacts and pre-sintered porous skeletons

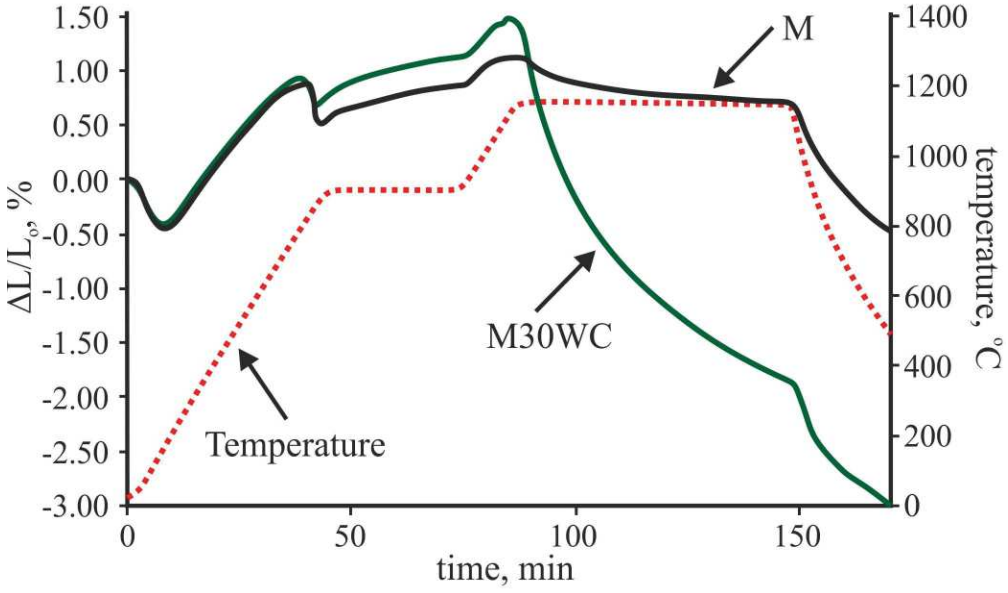

Fig. 7. Dilatometric curves recorded on heating the M3 and M30WC material to the sintering temperature

On the dilatometry curve of a change in length of green compacts made from M3 (Fig. 7), we can distinguish five stages of the sintering process:

1. in the first stage, changes in the length of samples are result mainly from their thermal expansion,
2. in the second stage of sintering, the shrinkage of the samples is mainly caused by the transformation of ferrite into austenite,
3. in the third stage during the isothermal heating, the temperature is equalized out in the entire volume of the sample, therefore thermal expansion works slightly, and it can also be presumed that there is a reduction of oxides on the surface of iron and HSSs particles. Dimensional changes can also be the result of the dissolution of M_6C carbides in the steel matrix [9,23],
4. in the fourth stage there is shrinkage of the samples caused by sintering in the solid state,
5. in the fifth stage, during the cooling of samples, the austenite transformation occurs, there is shrinkage of the samples caused by the products of this transformation and the cooling process.

As exemplified in Figure 7, marked specimen expansion followed by its rapid contraction has indicated that it takes place at temperatures between 1080 and 1130°C. Intermediate carbides, such as WC, partially dissolves releasing free carbon and tungsten. These chemical elements released from WC carbides react with steel matrix to produce new carbide phase with compositions similar to those of the normal primary carbides presented in high speed steel (M_6C type). Tur 62 X-ray diffraction (XRD) machine with Cu target (Kα, λ = 1.5406Å) were used to phase identification of as-sintered materials (Fig. 8).

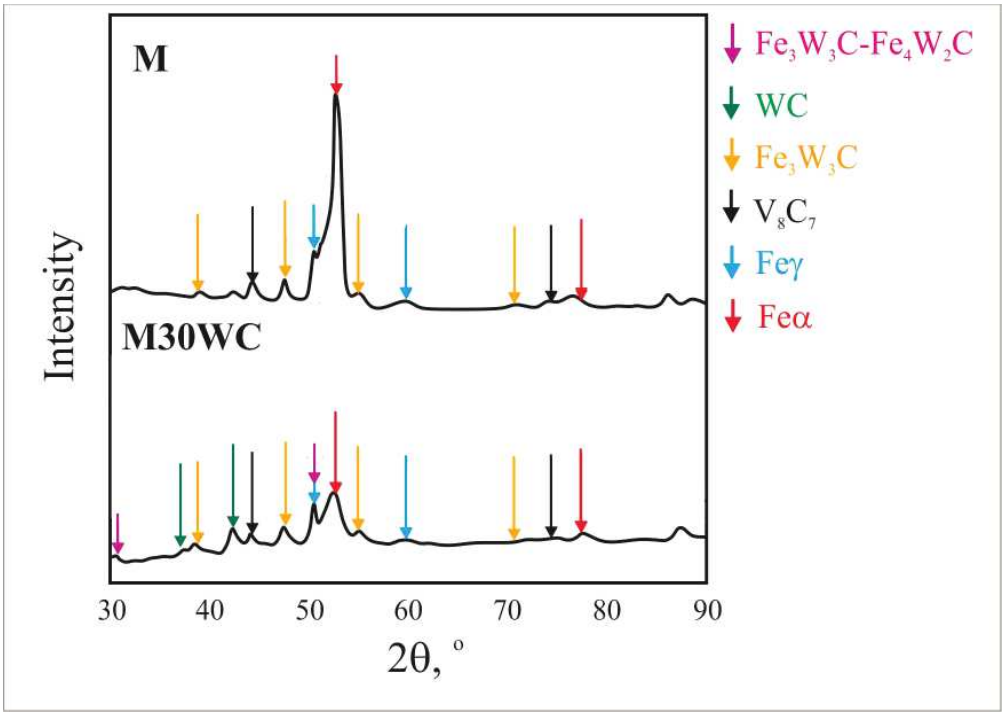

Fig. 8. X-ray analysis of porous sinter skeletons

The SEM microstructures of as-sintered porous skeleton before infiltration are show in Figure 9.

The SEM obserwations performed on the specimens M10WC and M30WC have exposed that the carbide phase are evenly distributed within the steel matrix. As it is apparent from Figure 9, WC dissolves nad then free tungsten and carbon reacts with the surrounding HSSs matrix and forms new, tungsten and iron-rich M_6C carbide grain boundary network during sintering of porous skeletons.

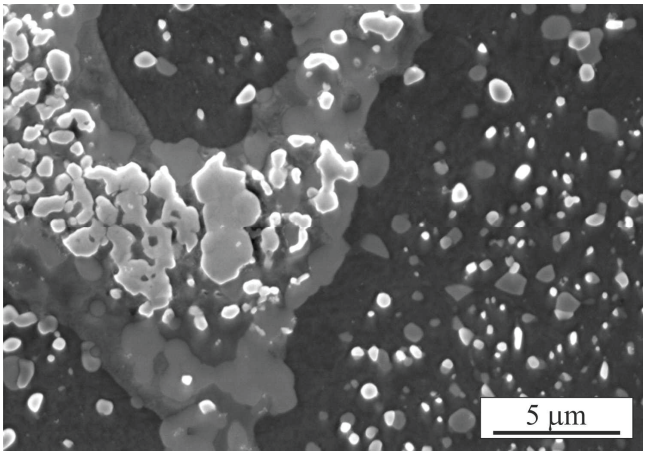

Fig. 9. SEM microstructures of as-sintered M30WC

The morphology of capillaries is one of the most important things influencing the progress of infiltration. Figures 10 and 11 shows the morphologies of capillaries in both green compacts and pre-sintered skeletons made from M and M50Fe powder mixtures.

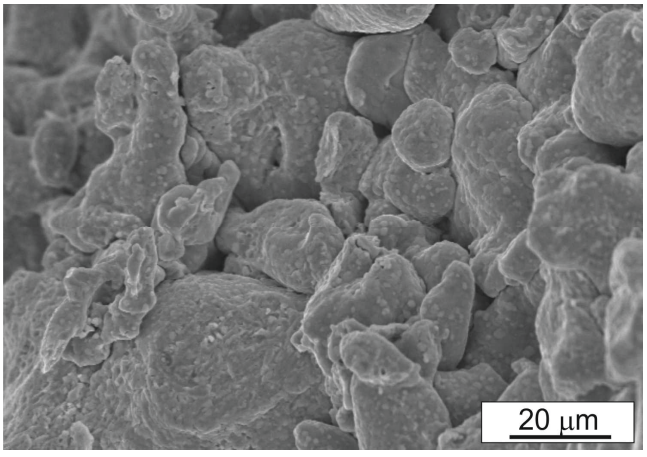

Fig. 10. The morphologies of capillaries in M50Fe green compact, SEM

Capillaries is a system of connected vessels whose shape in porous skeletons depends on the shape of the powder and the subsequent operations used for their concentration. It may be concluded from the SEM fractures of porous skeletons observations (Figs. 10 and 11) that the morphologies of capillaries are result from the powder characteristics (Figs. 1 and 2), such as powder particle size, morphologies of powder particles and its shapes. Irregular shape and porous microstructure of iron powder additionally change the character of capillaries (Fig. 11). The process of infiltration depends on the degree of oxidation of the capillary surface and the size of their radius, in order to reduce the oxides present on the surface of the powders, the process of pre-sintering of the porous skeletons part and the isothermal stop at 900°C before reheating to the infiltration temperature were used.

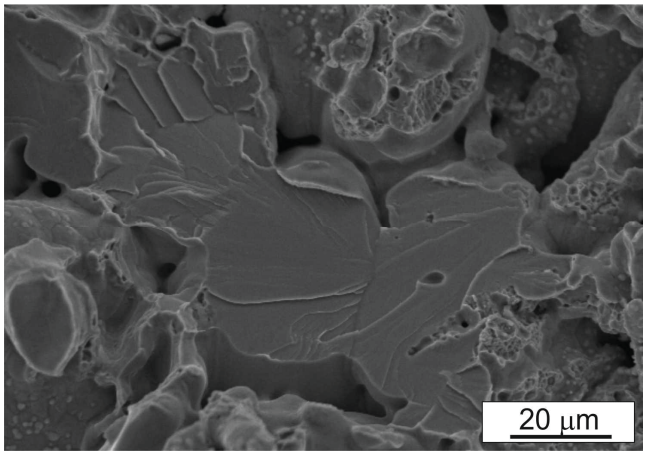

Fig. 11. The morphologies of capillaries in M50Fe as-sintered porous skeleton.

3.2. Properties of composites

The properties of composites obtained as a result of the infiltration of copper into porous skeletons largely depend on the methods of their production and the content of tungsten carbide. Selected properties of these materials are shown in Figures 12-15.

The measure of efficiency is the extent of infiltration of capillary filling S_w. This parameter is usually less than 100% because during the infiltration processes related to sintering with the liquid phase take place.

As seen in Figures 12 and 13 the molten copper was drawn into the capillaries of the porous skeletons, using only capillary forces, and allows materials to approach final density up to almost 100% of the theoretical value. If Cu excess remains on the sample surface – than it is mechanically removed by brushing. In all cases, the additions of tungsten carbides doesn't influence on the final density of the materials as compared with the base material. Direct infiltration of as-sintered skeletons M, M50Fe and M30WC with copper results in the highest densities. This may be result of deoxidation powder particle surfaces during sintering in vacuum – this leads to an impoverishment of carbon from steel matrix.

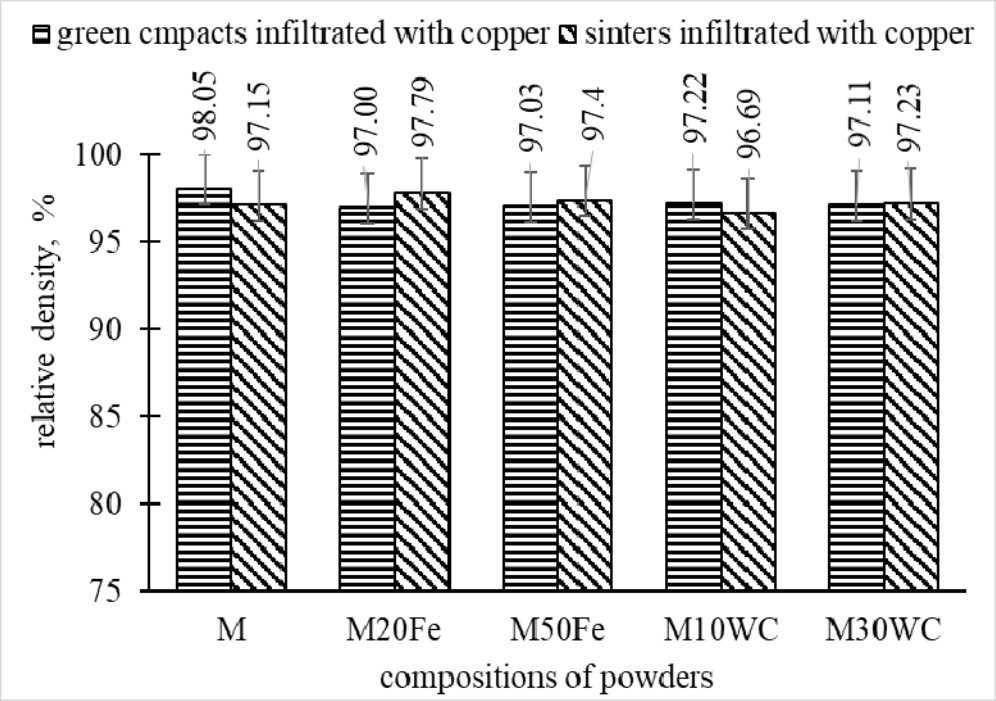

Fig. 12. Relative densities of as-infiltrated composites

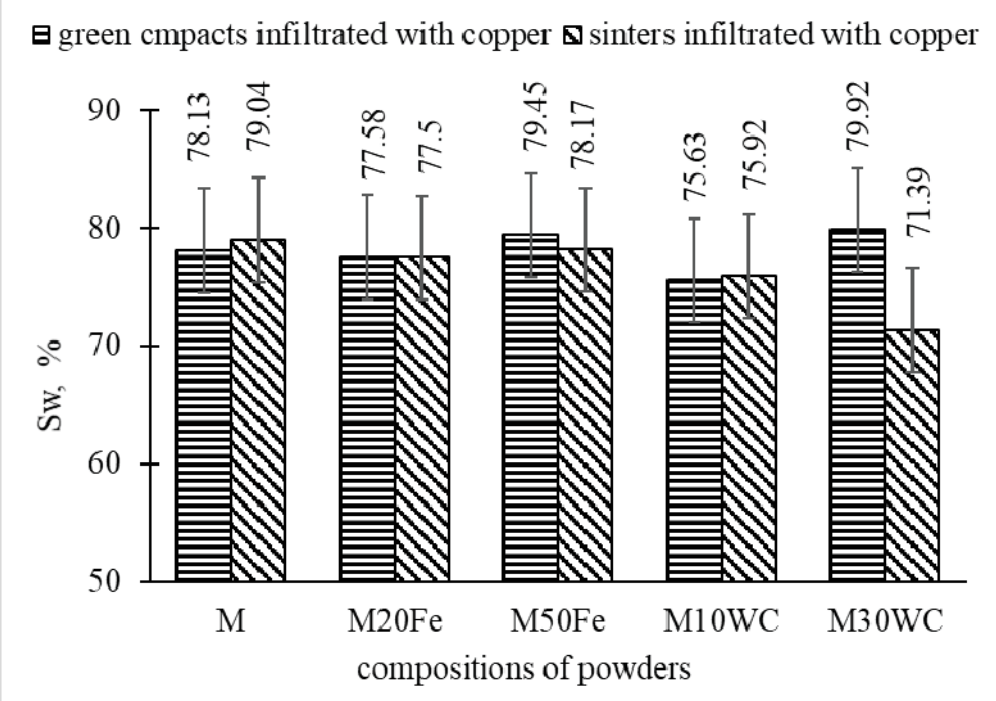

Fig. 13. The extent of capillary filling

Brinell hardness was tested using the Innovatest hardness tester; the test involved a tungsten carbides ball, 2.5 mm in diameter, and a load of 187 kgf. The average hardness values from 15 measurements on each sample and its standard deviations were determined.

The brinell hardness (Fig. 14) of the as-infiltrated composites decreases with the increased content of iron in the starting powder mix. The brinell hardness of the as-infiltrated composites increases with the WC addition. Slight difference in hardness between the materials obtained from the two manufacturing routes was observed, i.e. higher hardness was achieved after infiltration of green skeletons. This can be explained by reducing the carbon content during the initial sintering, which was used to reduce iron oxides.

Many mechanical properties of materials, mainly PM materials, such like: flexural modulus, stress-strain compensation and failure limits for bending all can be obtained by using a simple geometry sample of a 3-point bending te. In a 3-point bend test the rectangular sample is stressed and the corners undergo maximum stress and strain. Failure will occur when the strain or elongation exceeds the material's limits. The bending strength test (TRS) was carried out using the three-point bending method using a ZIM mechanical press.

The bending strength (Fig. 15) of HSSs based composites with iron additions does not seem to be affected by the different level of iron volume. The bending strength of composites after copper infiltration decreases with increasing content of WC (tungsten carbide) in the initial powder mixture. For the pre-sintering and infiltration with copper to M10WC and M30WC porous skeletons, there is an increase in bending strength; this can be explained by the dissolution of the WC additive carbide and the subsequent phenomena associated with it (sintered with an intermediate of the transition liquid phase, forming a new carbide phase).The M and M50Fe composites were heat treated (HT) according to the following scheme:

- austenitizing at 1050° C for 20 minutes and cooling in oil,
- tempering at 180 ° C for 2 hours.

Austenitizing and tempering of high-speed steel is carried out in a furnace that can be treated in a protective atmosphere, nitrogen atmosphere is used, after tempering the composites are cooled to room temperature in furnace cooler (system cooled by water).

Presented heat treatment is also the subject of a patent PL 397462 [32].

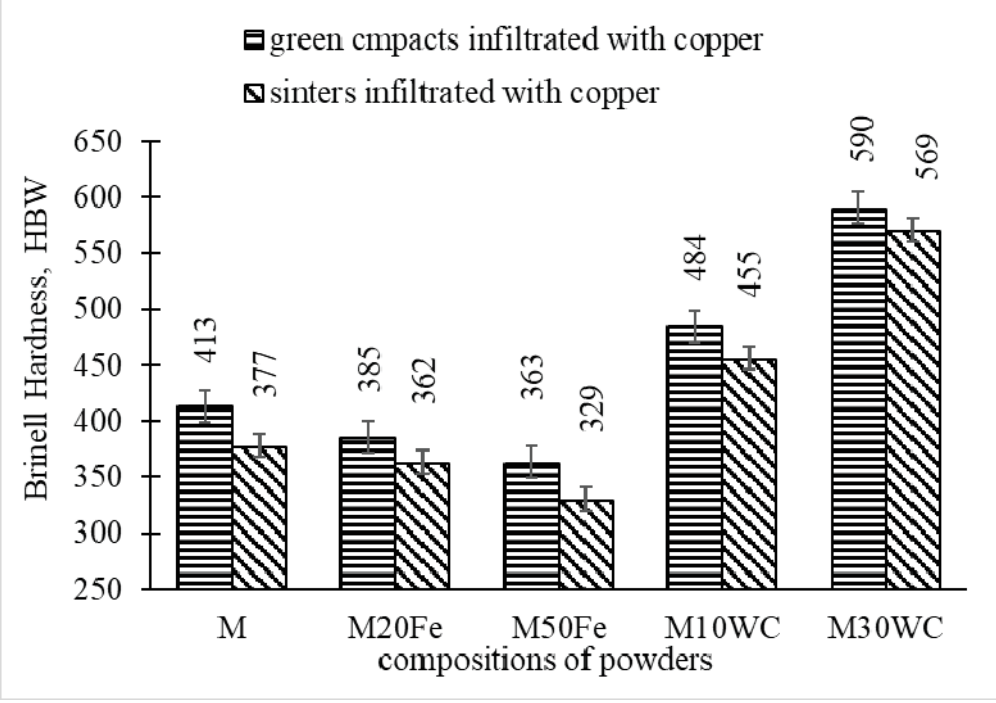

Fig. 14. The brinell hardness of as-infiltrated composites

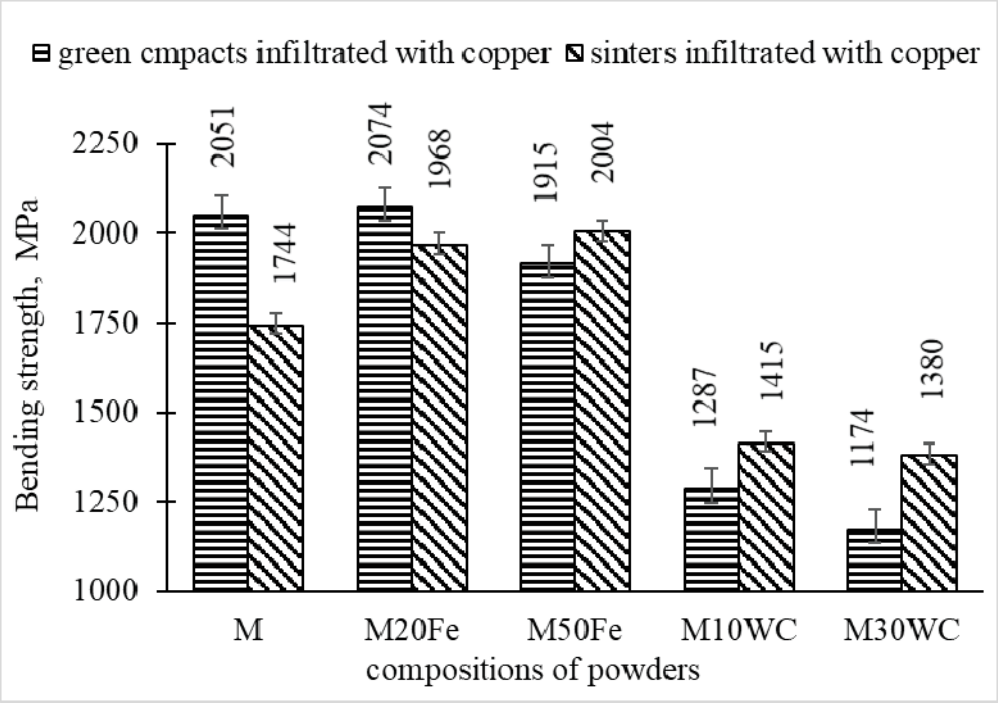

Fig. 15. The bending strength of as-infiltrated composites

Table 2.
The brinell hardness of M and M50Fe materials before and after heat treatment

The compositions of powders	After infiltration		After austenitizing and oil quenching		After tempering	
	$\overline{HB}$ [1]	$\sigma_{\overline{HB}}$ [2]	$\overline{HB}$	$\sigma_{\overline{HB}}$	$\overline{HB}$	$\sigma_{\overline{HB}}$
Infiltrated green compacts						
M	413	13.5	455	34	402	11
M20Fe	385	7.8	433	16	426	9
M50Fe	363	7.4	365	18	392	7
As sintered and infiltrated composites						
M	377	14	418	25	399	8
M20Fe	362	6.9	401	26	393	7
M50Fe	329	7.2	397	16	391	13

[1] – average brinell hardness
[2] – standard deviation of brinell hardness

The typical HSSs heat treatment is different, details are described in the publications [1,2,14].

A comparison of hardness results of heat treated materials is presented in the Table 2.

The application of such an unusual heat treatment results in changes in the hardness of the tested composites. As it could be seeing in the Table 2 the brinell hardness of composites increase after heat treatment. The greatest

attention should be paid to materials with iron addition after infiltration of copper into as-sintered porous skeletons.

The tests of the microhardness distribution in iron particles were also carried out. The results are summarized in Table 3.

Table 3.
The microhardness of iron particles after HT

Measuring area inside iron particles	**$HV_{0.065}$**	σ_{HV}
Area near the grain boundary between iron-high speed steel	466	24
The centre of the iron particle	321	10
Area near the iron-copper border	248	6

The test results presented in Table 3 show that the hardness changes as a function of the distance from the grain boundary of the high speed steel to the inside of the iron particle. The lower hardness can be measured at the copper - iron grain boundary area - this is due to the failure of diffusion in this area of alloying elements, including carbon, from steel matrix.

3.3. Microstructures of HSSs based materials with iron additions

The infiltrated specimens were subjected to microstructural examinations by means of both scanning electron microscopy (SEM) and transmission electron microscopy (TEM). Typical SEM microstructures of a copper infiltrated pre-sintered skeleton are shown in Figures 16-18.

It can be seen that the microstructure of the M3 type 2 HSSs based composites contains a steel matrix with finely dispersed different types carbides and copper regions between steel particles. When we look at the HSSs matrix we could see the M_6C and MC types carbides uniformly distributed in steel matrix (Fig. 17) [29,30]. In order to identify types of carbides, they were tested for their chemical composition by the EDS point method. The results of this investigations are shown in Figure 17.

Results of the chemical point analysis of HSSs particles shown the existence of the two types of carbides: M_6C and MC as well as the existence of ferrite and austenite (Fig. 8) in as-sintered matrix of HSS. Most Fe is found in the matrix and grey M_6C carbides (in wwhich there are also dissolved Mo, W, Cr), while V and W are identyficated in the whitish MC carbides. (Fig. 18). Confirmation of these tests are also analyses carried out using the transmission electron microscope (TEM).

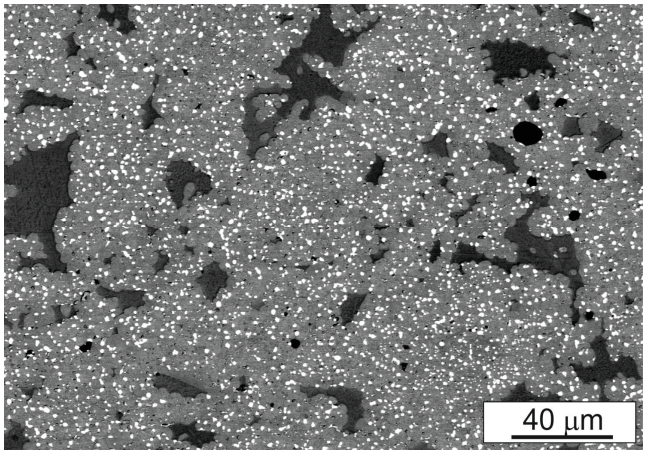

Fig. 16. Microstructure of M3/2 HSS based composites infiltrated with copper

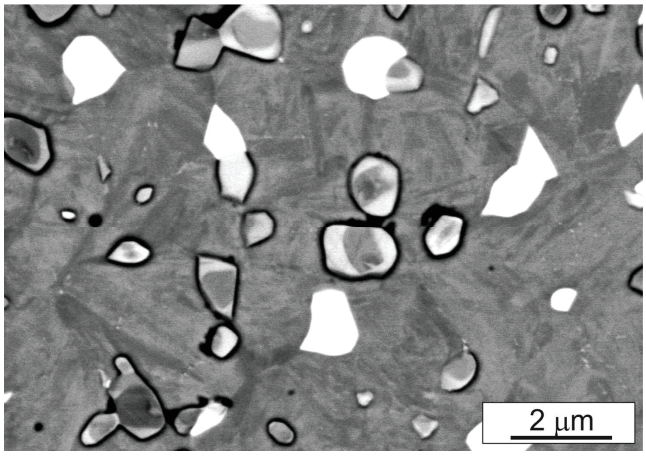

Fig. 17. The distribution of carbides inside of HSS matrix, SEM

The mechanical properties of as-sintered and as-infiltrated composites M50Fe (Figs. 14 and 15) show that after infiltration of as-sintered porous skeletons it is observed that the hardness does not decrease as if it resulted from high volume of iron in this type of materials. It can be explained by the diffusion of alloying elements from HSSs matrix to iron particles during sintering which consequently leads to a reduction of steel matrix properties, but increasing of iron particles properties.

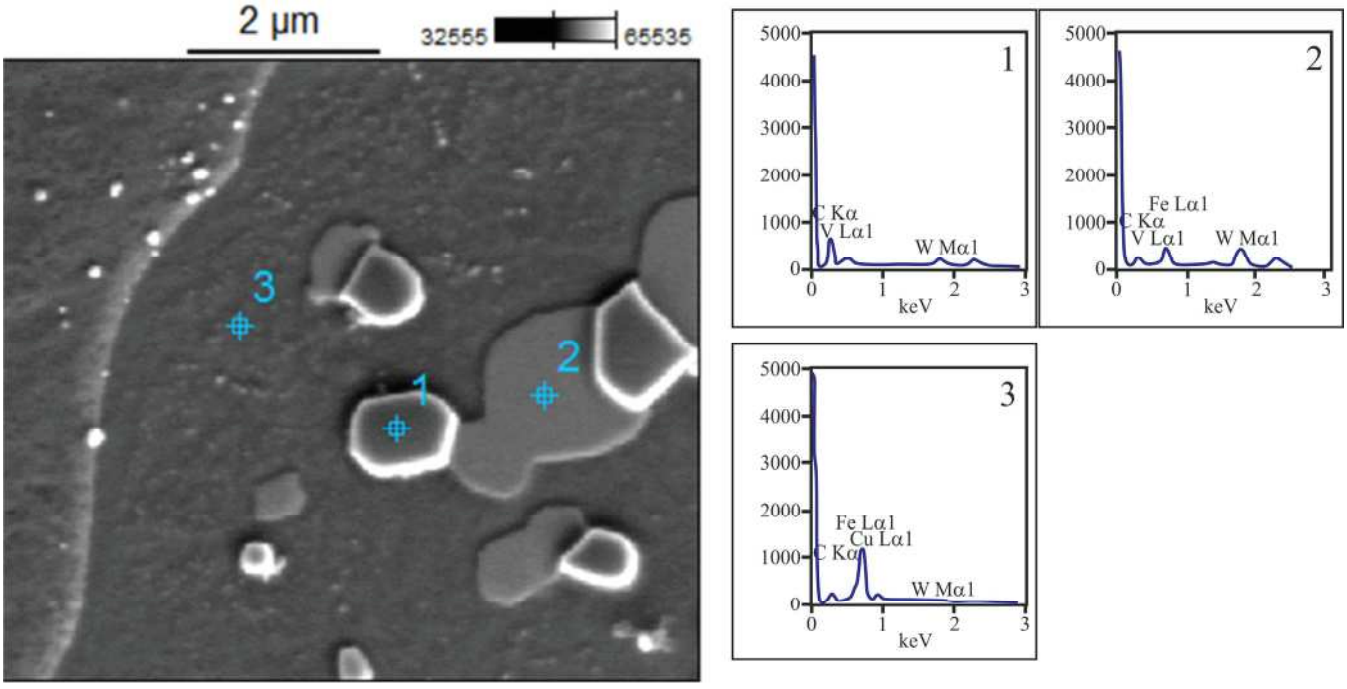

Fig. 18. The microstructure HSSs matrix of sintered and copper nfiltrated M composites: 1 – MC carbides, 2 – M6C carbides, 3 – HSSs matrix, SEM

This diffusion of alloying elements during sintering before infiltration was analysed by SEM and EDX methods. Figure 19 shows typical microstructures of M50Fe materials produced by infiltration of as-sintered porous skeletons. Linear analysis of distributions of elements at the interface of iron – copper – high speed steel particles in M50Fe materials after infiltration are show in Figure 20.

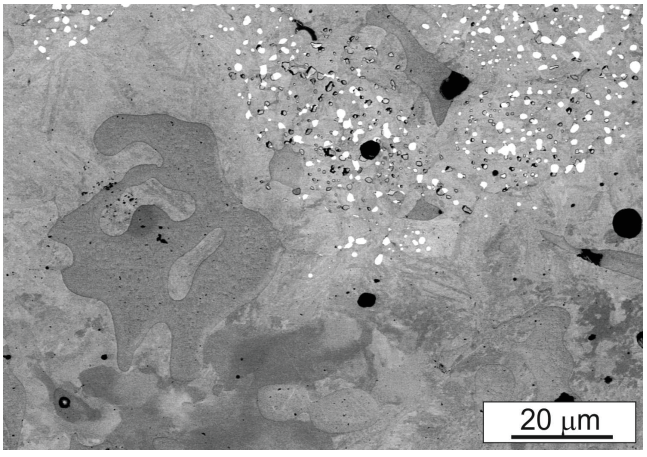

Fig. 19. The microstructures of M composites with 50% Fe additions, SEM

It is known that after heating above 900°C the $M_{23}C_6$ carbide begins to dissolve and continues this up to temperature of 1100°C (but there is not of $M_{23}C_6$ type of carbides in M3 type 2 HSS). The solution of M_6C carbides existing in M3 type 2 HSS begins between 1100-1150°C, MC carbides barely dissolves at all. From Figure 21 it can be seen that there is a diffusion of carbon, molybdenum, chromium, and manganese from steel to the additions of iron particles. These chemical elements diffused from the high-speed steel die and partially dissolved M_6C carbides that were near the high-speed steel boundry. Diffusion of these elements during sintering of materials with different iron addition is enhanced by the presence of carbon in solution [7], during sintering at temperatures 1150°C M_6C type carbides started to dissolves and carbon diffuse to austenitic matrix of HSSs and to iron particles. There is also bidirectional diffusion between copper and iron, copper also diffuse to HSSs matrix. The solubility of copper at this temperature in iron is about 6%, in steel due to the presence of alloying elements in the matrix are smaller and estimated at about 4%.

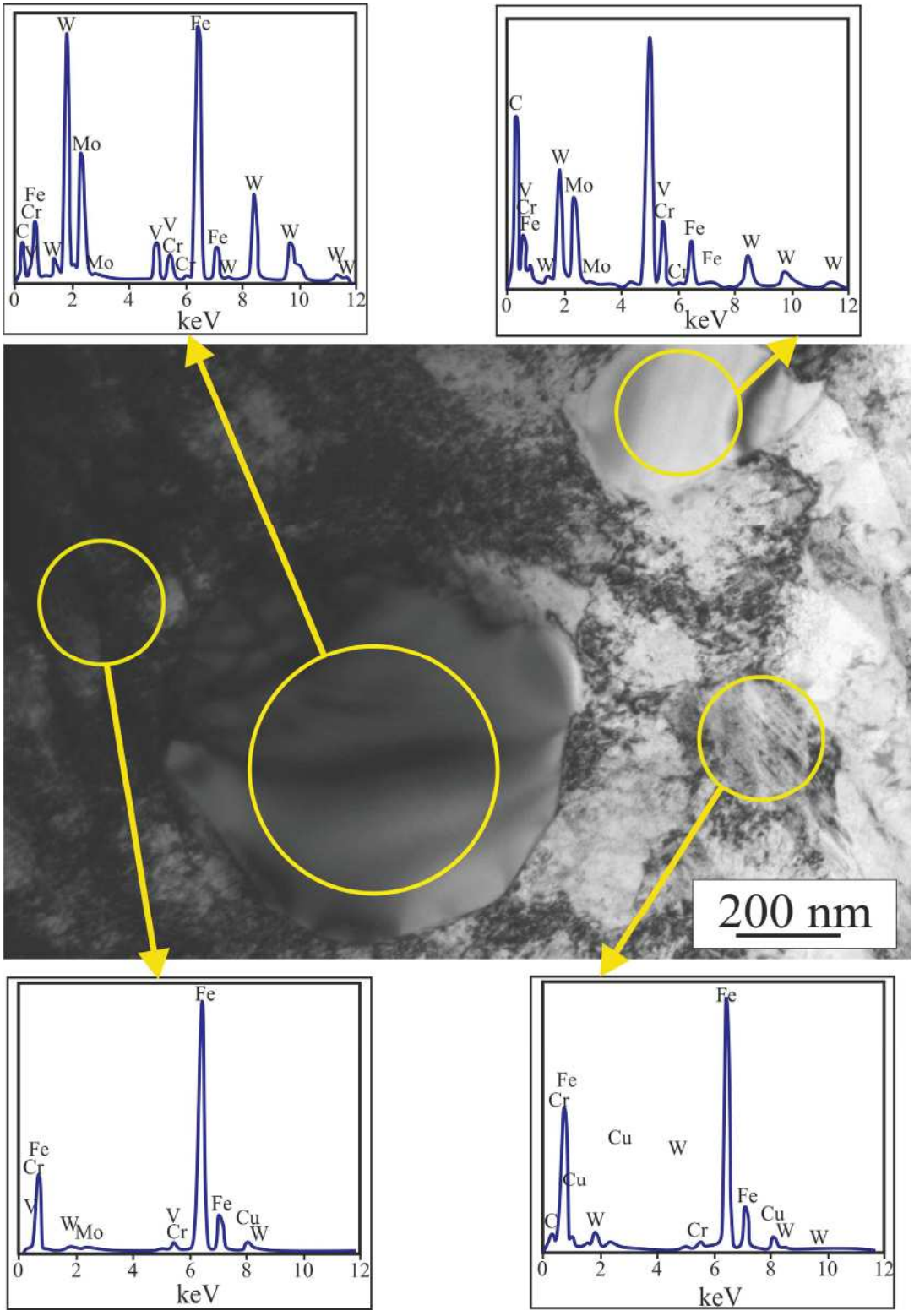

Fig. 20. The microstructure of HSSs matrix of sintered and infiltrated with copper M composites: 1 – MC carbides, 2 – M6C carbides, 3 – HSSs matrix, TEM

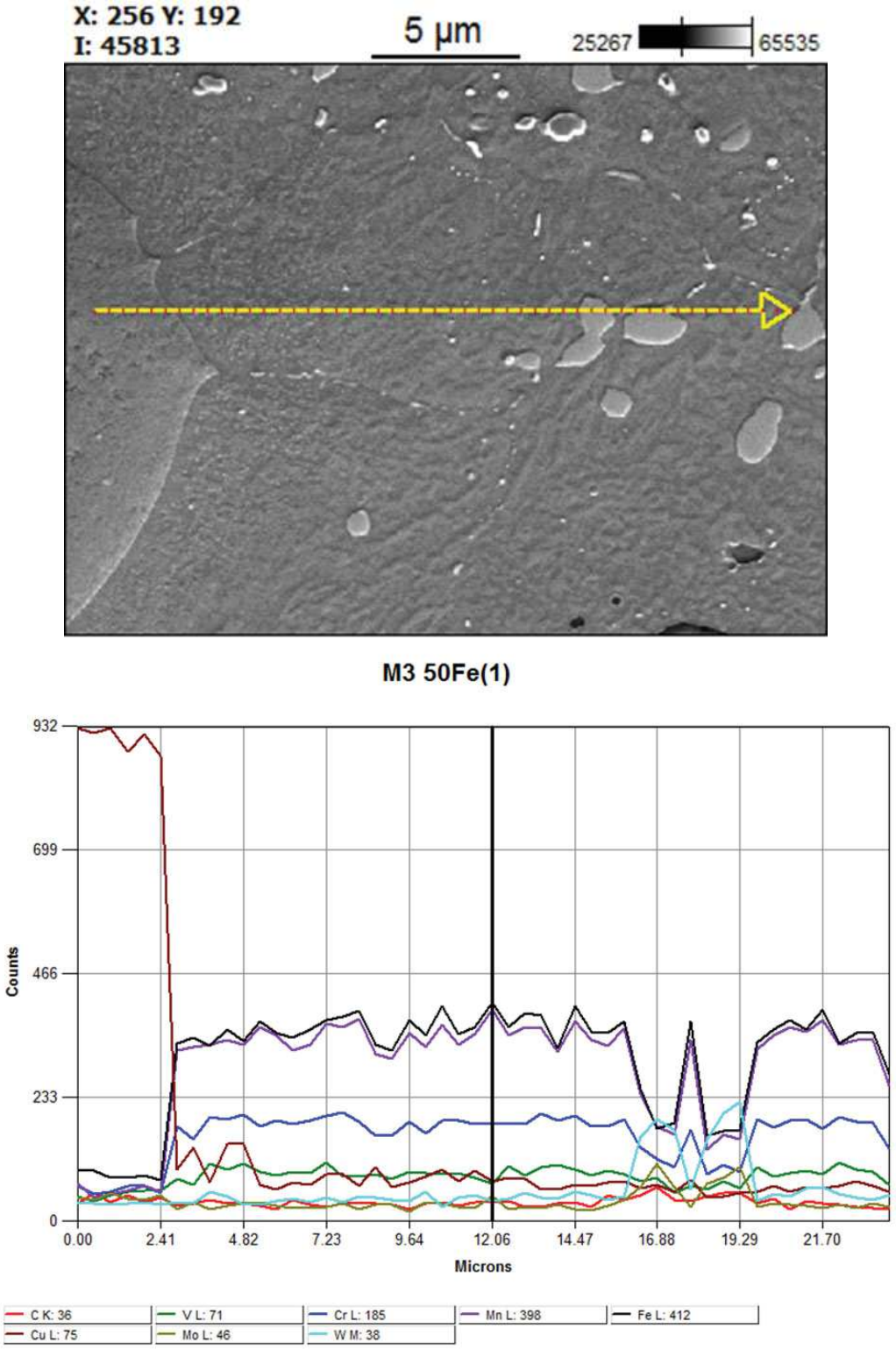

Fig. 21. The microstructure of HSSs matrix and the qualitative EDX linear analysis

Analysing the hardness results obtained for materials after heat treatment allows us to assume that further changes in the microstructure occur in the materials under study. microstructure of materials after infiltration and heat treatment are presented in the following Figures.

Looking closer, especially to the iron areas at the contact grain boundary with high speed steel, the appearance of a lamellar microstructure characteristic of martensite can be observed. Typical microstructure with this effect is show in Figure 21.

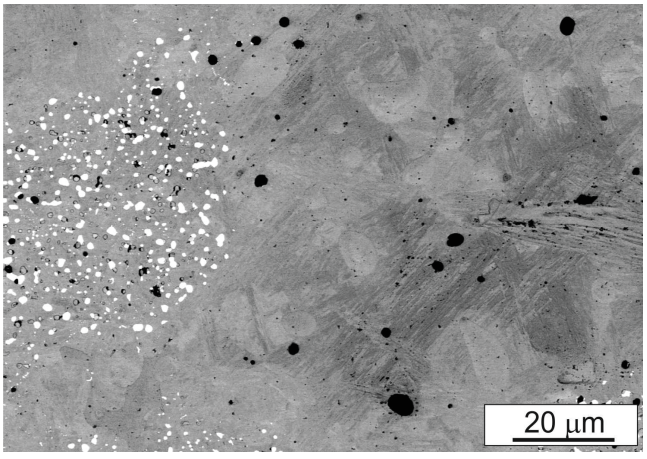

Fig. 22. Microstructures of M50Fe composites after HT

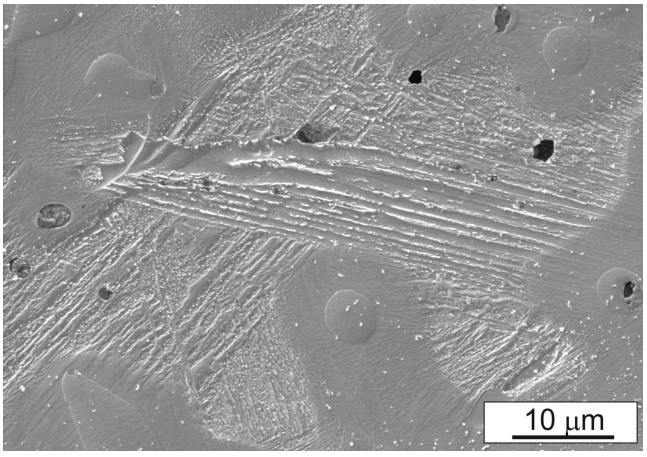

Fig. 23. SEM microstructure of the grain boundary HSS-iron

They analyse the microstructures of the M50Fe material shown in Figures 22 and 23 after infiltration and heat treatment, further reducing the number of carbides in the steel matrix close to the iron border. This allows further diffusion of alloying elements from steel to iron, including carbon and result in microstructural changing during quenching. Another observations of microstructures were carried out using a transmission electron microscope. The results of this observations are shown in Figures 24 and 25.

Figure 24 shows the grain boundaries area between iron and copper particles. A characteristic feature of this particle system is the presence of iron particles inside the iron particles of nanometre size (below 100 nm). These precipitates are concentrated near the grain boundary, and they are distributed evenly. Precipitations of these copper particles is caused by the interdiffusion of these elements, however, there is a significant difference in the solubility of these elements. The solubility of these elements strongly decreases to the room temperature, this allows the precipitation of copper nano precipitants inside iron particles, probably during tempering. The STEM chemical composition analysis of the precipitates were also carried out, the results of the analysis are presented in the Figure 26.

The linear analysis of the distribution of elements confirmed the fact, that these precipitates consist mainly of copper. This microstructural effect is sometimes called “coffee effect”. This is an additional effect that positively affects on the increasing of the properties of tested materials (Figs. 14 and 15).

3.4. Microstructures of HSSs based composites with WC additions

The effects of the addition of tungsten carbide on the microstructure of as-sintered porous skeletons before infiltration are presented in chapter 3.1. It is known that carbides, such as WC, partially dissolves in this type of chemical and thermal combination and react with steel matrix to produce new carbide phase with compositions similar to those of the normal primary carbides presented in high speed steel. It takes place between 1080 and 1130°C. The main question is about as-infiltrated green compacts. They were only near 20 ~ 25 minutes in this range of temperatures and also liquid copper penetrating capillaries. The SEM microstructures of M30WC composites produced by direct infiltration of green compact are shown in Figure 27.

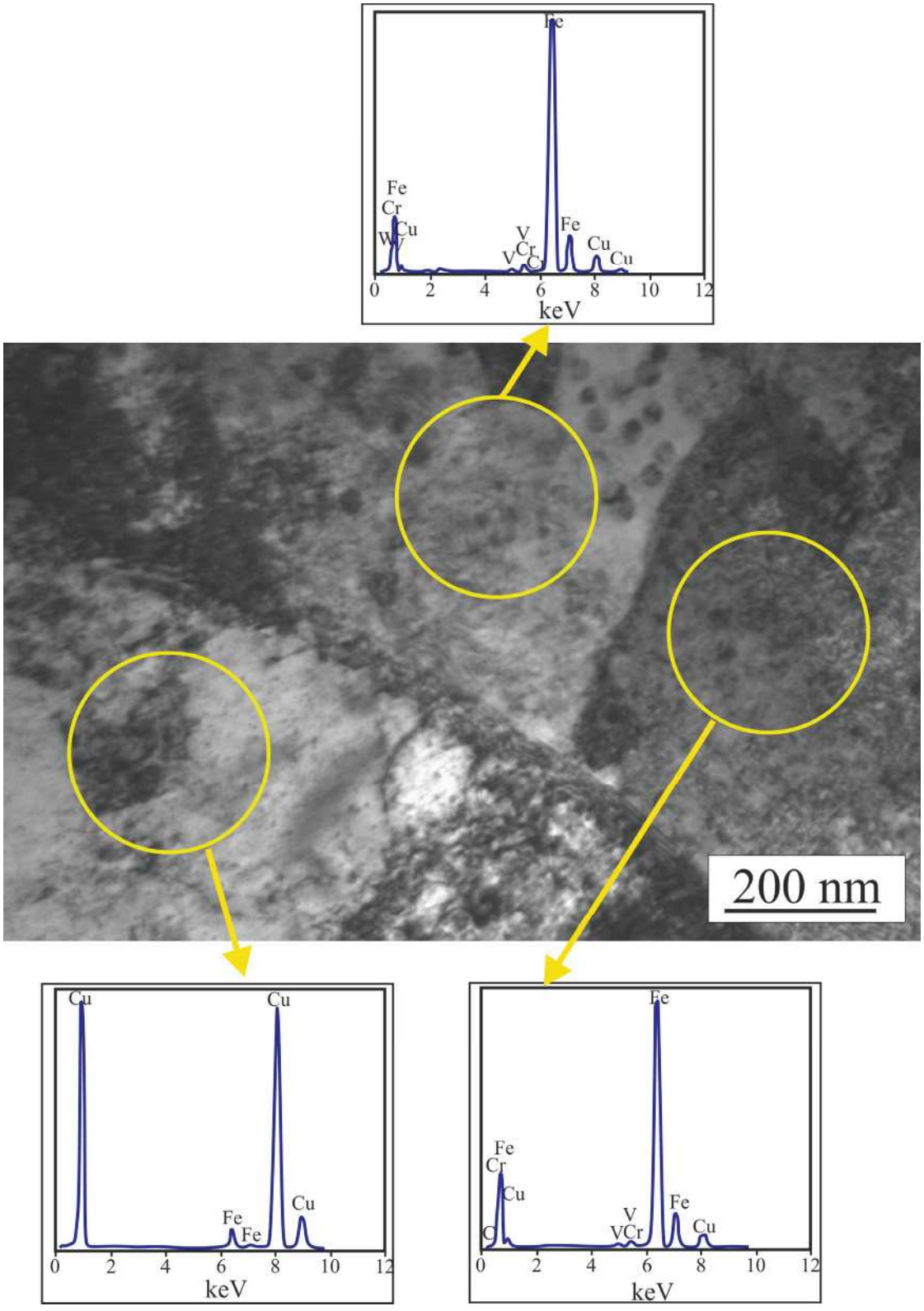

Fig. 24. TEM microstructure M50Fe materials after HT

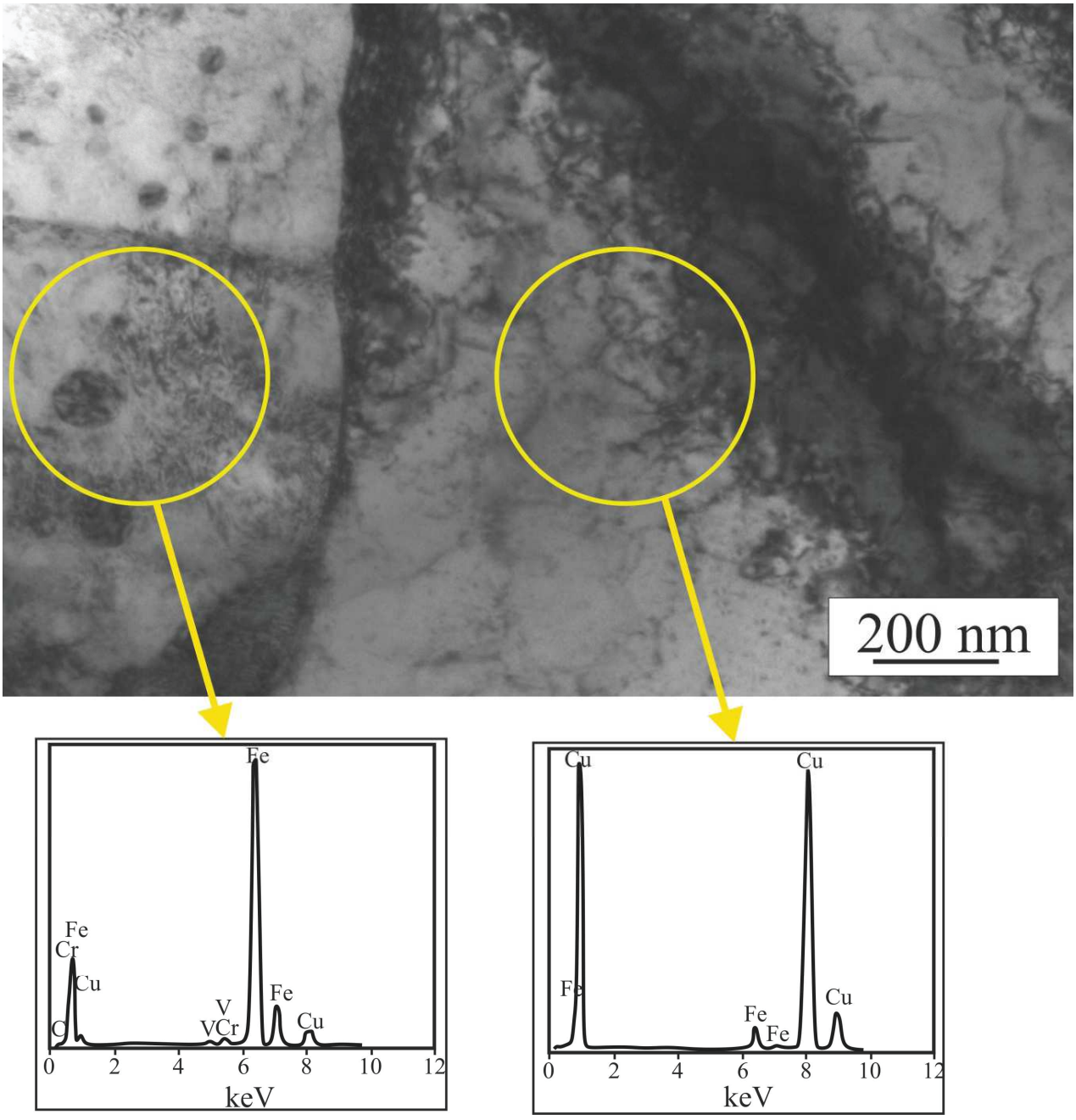

Fig. 25. TEM microstructure M50Fe materials after HT

As it can be seen in Figure 27 the effect of WC reaction with HSSs matrix is much lower than in M30WC composites produced by infiltration of as-sintered materials. It could be seen that there are the coating around the WC carbide additive, but it is smaller than in M30WC produced by infiltration of as-sintered materials, another conclusion are that the WC carbide particles are separated – compared to those present in the microstructure of as-sintered M30WC composites (Fig. 28).

To identify phenomena at the HSS-WC contact interface, there were chemical composition analysis using SEM. The results are shown in Figure 29.

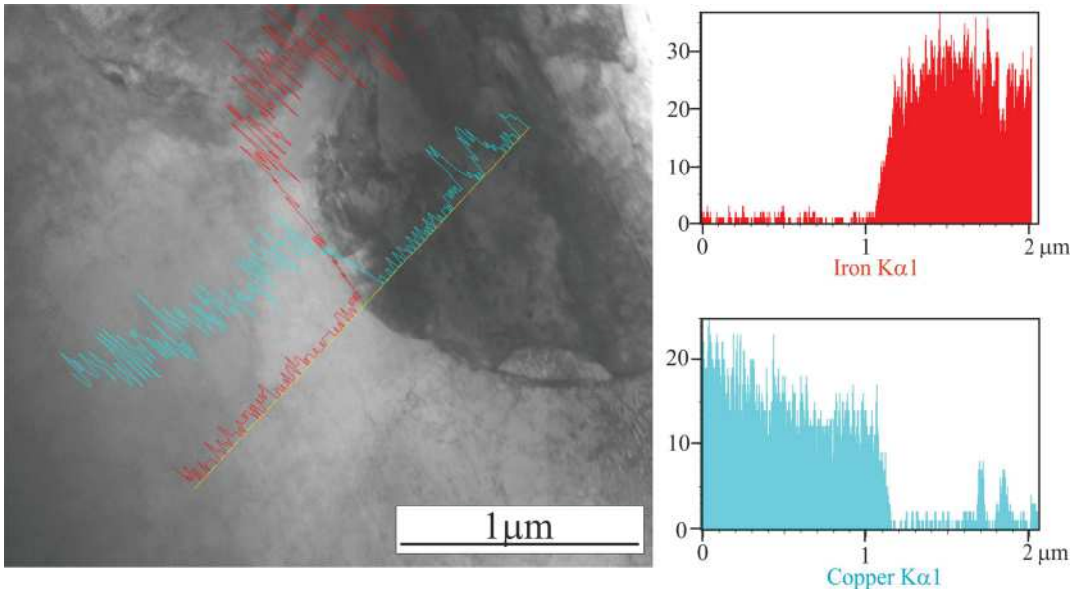

Fig. 26. The microstructure of large copper precipitates inside iron particles and linear analysis of element distributions TEM

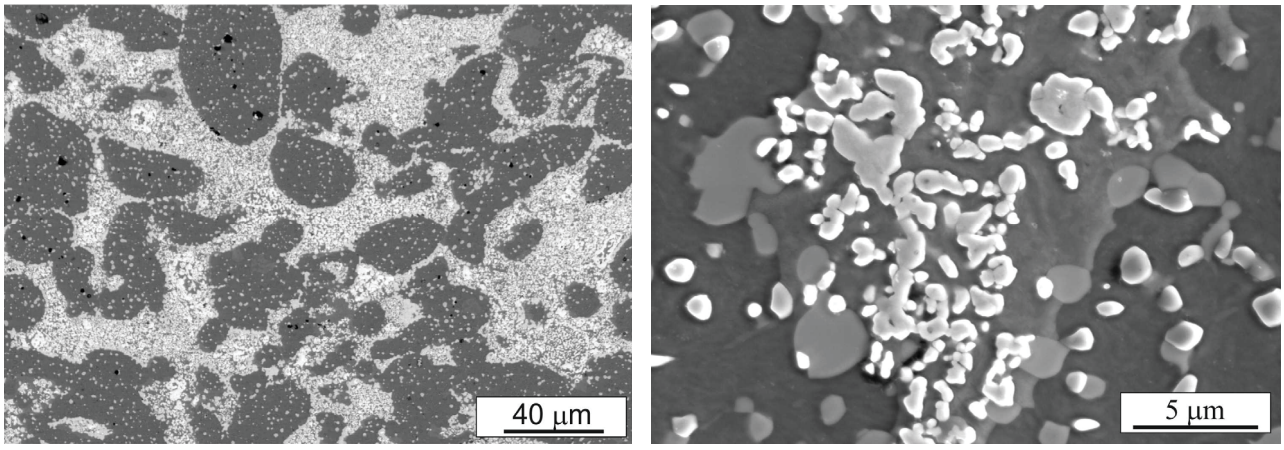

Fig. 27. SEM microstructure of as-iniltrated green compact of M30WC

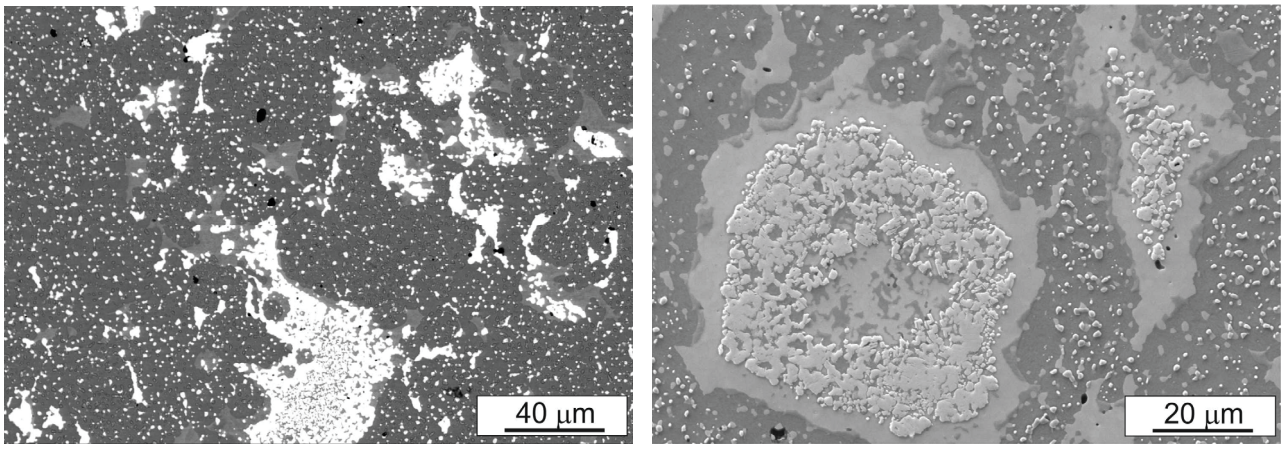

Fig. 28. SEM microstructure of as-infiltrated composites M30WC produced by infiltration of as-sintered porous skeletons

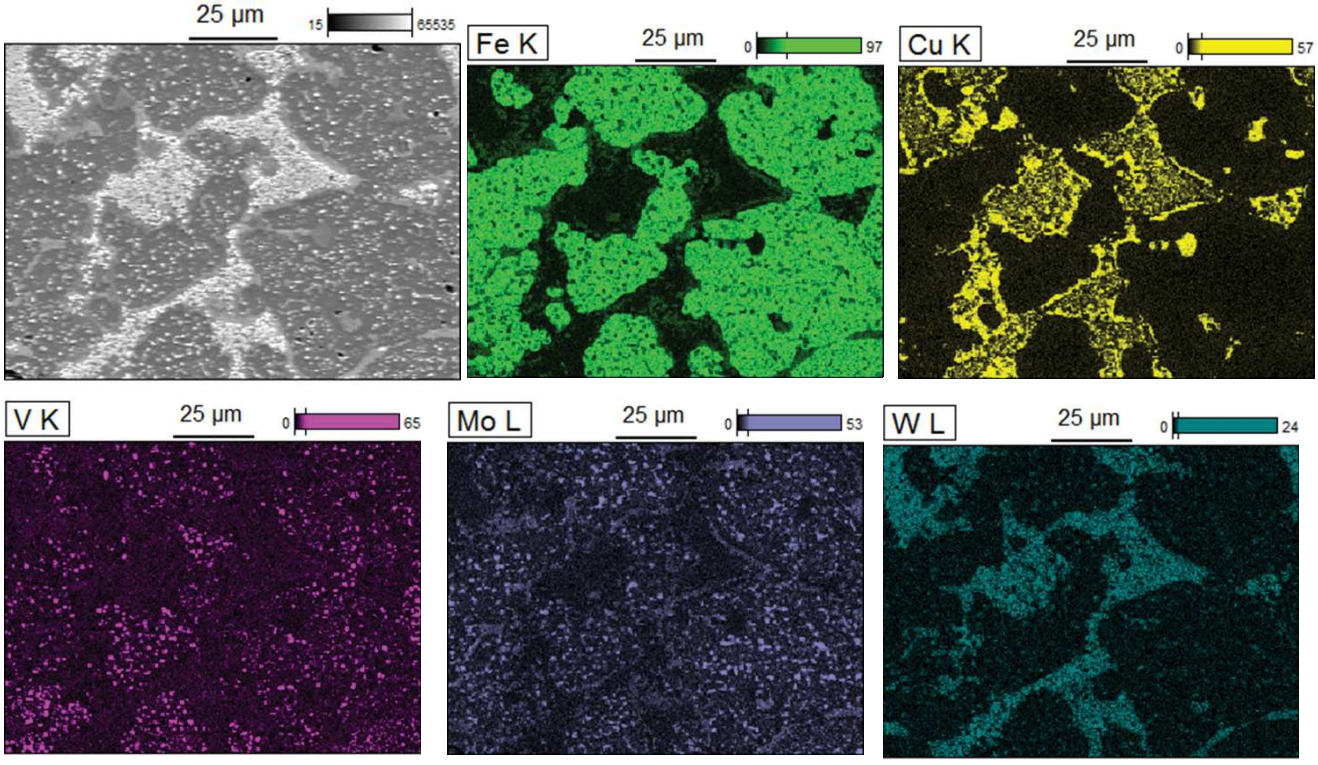

Fig. 29. SEM microstructure of as-infiltrated green compact M30WC and Fe, Cu, V, Mo, W distribution map

Table 4.
Average chemical composition of different types of carbides contained in high-speed steel [25]

Carbide type	W	Mo	V	Cr	Fe
M_6C	33.9 ± 3.9	23.8 ± 2.6	3.8 ± 0.9	4.3 ± 0.7	32.5 ± 1.3
MC	19.9 ± 6.7	12.7 ± 3.3	49.2 ± 5.2	4.2 ± 2.0	3.1 ± 1.8

The carbides formed at powder processing etap aretakes palce the formation of the secondary carbides, which are fine or ultrafine [28,33]. Typical analysis of carbides in HSSs matrix shows that the MC carbide are mainly VC carbides and sometimes contains very small amounts of iron and consists essentially of tungsten and molybdenum. The amounts of tungsten and molybdenum depend of the steel composition because W and Mo are used interchangeably. M_6C type carbides are rich in tungsten, molybdenum, and iron, the amounts of vanadium and chromium dissolved in this carbide correspond approximately to the quantities present in the steel grade which are used (Tab. 4).

XRD pattern of as-sintered specimens shown in Figure 8 shown the existence of the main carbides MC and M_6C as well as the existence of ferrite and austenite in M material. The XRD patterns of as-sintered M30WC samples illustrates the existence of the main carbides M_6C (both types: Fe_3W_3C and more stechiometrically complicated Fe_3W_3C-Fe_4W_2C) and MC (WC and V_8C_7) as well as the existence of ferrite and austenite. It should be noted that the intensity of the Fe_3W_3C-Fe_4W_2C peaks in pre-sintered samples can be explained by the dissolve of the tungsten monocarbide and HSSs matrix. In the ICSD and ICDD databases of the data crystallographic and the data of the diffraction pattern, respectively, is possible to find many types of carbide with different stoichiometry. The carbides, mainly M_6C type can show many crystalline structures and it is no easy to exactly identify its chemical compositions.

The main difference in the identification of the new precipitated carbide (M_6C) is that it forms outside the steel matrix. From Figure 29 it is evident that there are only small amounts of new M_6C type carbides between HSSs and WC additions. It mainly copper infiltrates to the areas at the boundary between WC and steel. This grey area in microstructure of M30WC produced by infiltration of green compacts are copper layer. Infiltration in a vacuum also provides the possibility of copper penetration into the interior of agglomerates and even their separation – as shown in the Figure 29. From Figures 28 and also 29 it is evident that during infiltration of green compacts with copper there are no conditions for the formation of a carbide layer at the HSS-WC boundary as it happens in pre-sintered porous skeletons. When using a mixture of HSSs and WC powders, new M_6C carbide is formed outside the steel matrix, precisely at the contact boundary between these two components. The EDS analysis was carried out pre-sintered skeleton M30WC infiltrated of copper to illustrate the chemistry of this carbides.

Metal carbides popular on the market, such for example WC used in the presented investigations, usually react with the steel matrix, lead to the formation of new carbide phases with compositions similar to ordinary primary carbides present in most high-speed steels, eg M_6C (Fe_3W_3C and Fe_3W_3C-Fe_4W_2C). This analysis (Fig. 30) does not show the presence of alloying elements from steel, other than carbon and iron in this new carbide. To accurately determine the distribution of elements in the studied area, maps of the distribution of elements were also made.

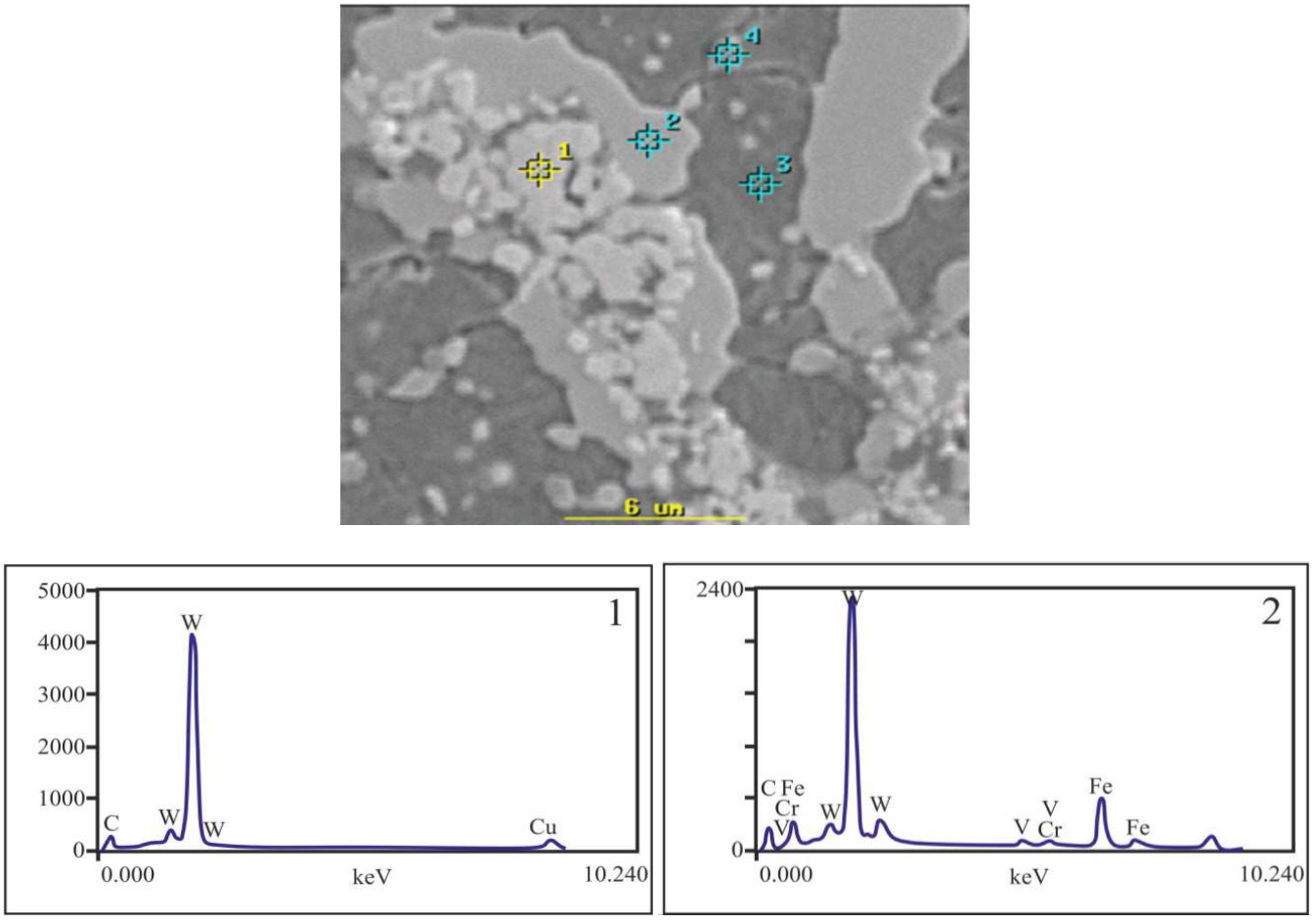

Fig. 30. The microstructure of M30WC composites produced by direct infiltration of as-sintered composites and point analysis of chemical compositions

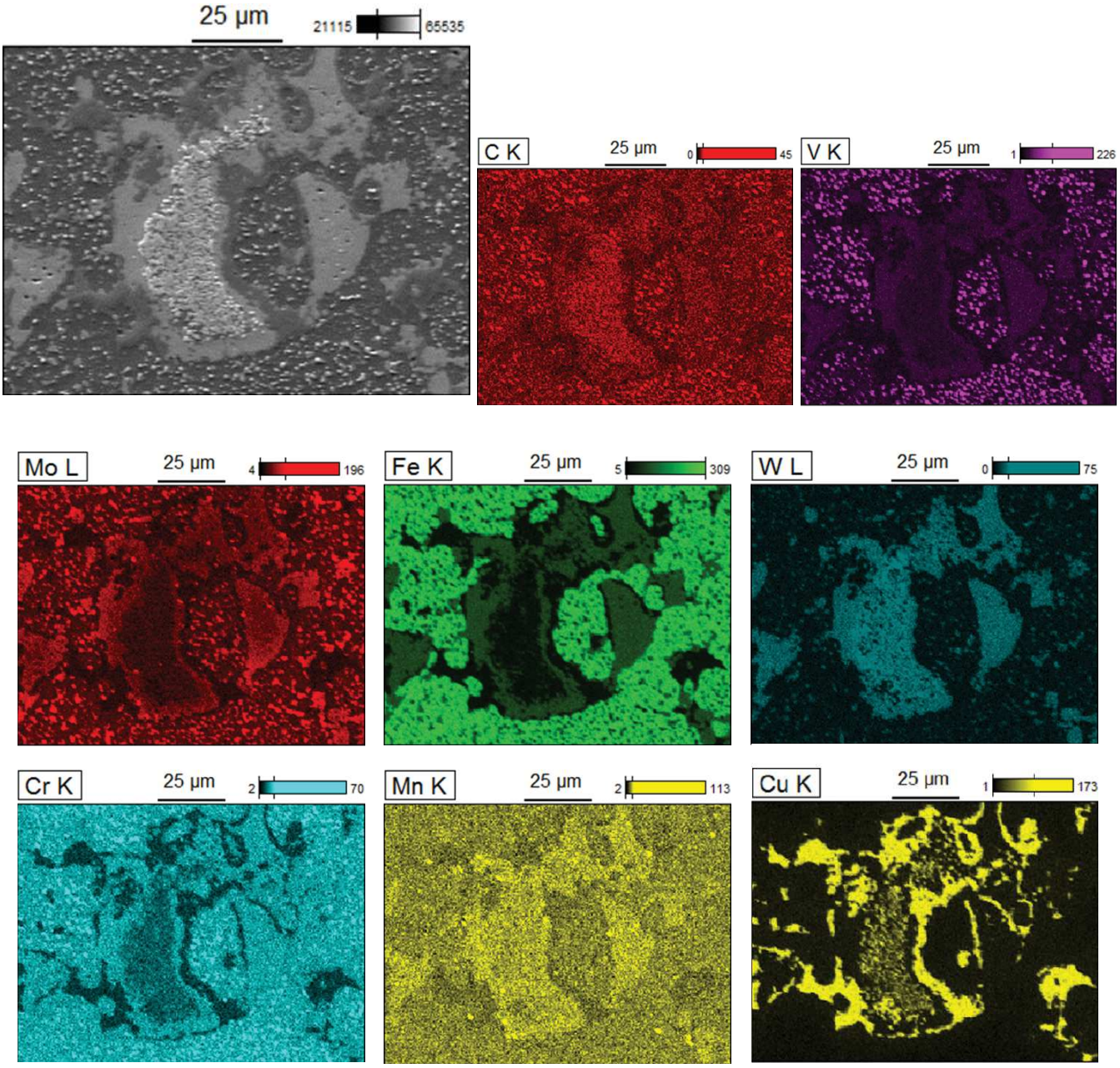

Fig. 31. Microstructure and distribution maps of C, V, Mo, Fe, W, Cr, Mn, Cu, SEM

The map of the distribution of elements in the microstructure presented in the Figure 31 shows that in the area of the newly established carbide M_6C there are alloying elements, which diffused from the HSSs steel matrix, and took up free positions in the crystalline lattice characteristic for the complex M_6C type carbides. Stoichiometrically recognized carbide from XRD analysis is described by **Fe_3W_3C-Fe_4W_2C** formula**.** The described carbide formula (M_6C type) does not include other elements dissolved in it, such as: Mo and Cr. Analysis of the presented maps of elements distribution shows that the amount of diffusion elements is much lower than in carbides inside the steel matrix (Fig. 30).

Table 5.
Carbides average chemical composition present in high-speed steel and M30WC as infiltrated composites (own research)

weight %	C	V	Cr	Fe	Cu	Mo	W
M_6C inside steel matrix	4.36±0.34	2.10±0.15	3.02±0.52	30.18±2.74	0.00	22.91±1.87	37.42±1.52
M_6C on WC/steel grains boundary	4.77±0.40	1.60±0.17	2.48±0.37	24.50±3.37	3.60±0.12	8.36±0.78	54.71 ±4.12

Average chemical composition of carbides M_6C type present in high-speed steel and M30WC composites produced by direct infiltration of as-sintered porous skeletons shows that there are some differences in chemical compositions of this M_6C carbides formed in various conditions (Tab. 5). As it might be expected with regard to the proposed carbide formula Fe_3W_3C-Fe_4W_2C it is not entirely accurate, there are dissolved elements in this carbide, besides tungsten and iron. These elements are: V, Cr and Mo, however, their participation is much smaller than in the classic M_6C carbide identified in the steel matrix. These investigations once again confirm the possibility of dissolving M_6C carbides contained in the steel grains, at the boundary with active additives, which allows the diffusion of alloying elements to iron (as described earlier) and to the newly formed carbide at the WC/HSS boundary. The analysis of the X-ray diffraction patterns presented in this work (Fig. 8) indicates that there are deviations of the chemical composition of the carbides. This fact can be attributed at the atomic substitutions in the crystalline structure and stoichiometry deviations. This studies show how difficult it is to accurately identify the kind of carbide knowing its type (M_6C).

After analysing the chemical composition of the newly created carbide, it could be presented in a simplified way: **$(Fe, Mo, Cr)_3(W)_3C$**.

The carbide agglomerations are observed due to the Turbula T2F system used for mixing the powders; they could be avoided by using a more efficient mixing system such as the classical ball mill.

3.5. Tribological properties

The measurements of the wear resistance and friction coefficient permit classification of the as-infiltrated composites with respect to their tribological properties. The M, MXFe and MXWC samples were used for wear tests performed by the block-on-ring wear tester. The tests were carried out at room temperature, keeping a relative humidity below 35%. All the specimens were polished according to ASTM standards to an average roughness of Ra = 1 μm. The results are presented as graphs of the mass loss (Fig. 32).

Direct infiltration of porous skeletons produced only by compacting with copper results in the highest wear resistance and lower friction coefficient of the as-infiltrated M, M20Fe and M50Fe materials. Comparing the wear resistance (represented by the loss off mass) of the composites obtained by direct infiltration of the green compacts and infiltration of the pre-sintered skeletons, it is obvious that the pre-sintered M50Fe compositions show 12-13 times bigger loss of mass than the green compacts containin iron and infiltrated with copper. This is result of the diffusion of carbon and alloying elements from steel to iron particles during sinterin and therefore a reduction in the tribological properties of high-speed steel particles due to reduction of M_6C carbides volume. Increasing the content of alloying elements in iron does not compensate for this loss of tribological property of steel. Additives 30% WC for high-speed steel and copper infiltration increase the resistance of these composites compared to the basic material (M infiltrated with copper).

The average coefficient of friction for the tested composites is at low level for metal alloys and amounts to:

- 0.380 ± 0.098 for M composites,
- 0.320 ± 0.080 for M20Fe and M50Fe composites,
- 0.370 ± 0.040 for M10WC and M30WC composites.

Addition of Hoganas iron powder and WC carbides result in decreasing in the friction coefficient of materials obtained from direct infiltration of green compacts. In MFe materials it could be explained by the presence of iron inclusions in the microstructure of as-infiltrated composites, which impart good sliding properties of materials with iron additions, but additions of WC carbide changes the mechanisms of wear of this type of materials, the share of abrasion increases.

The tribological tests were also carried out for materials with iron addition after heat treatment. The comparison of mass losses of tested materials before and after heat treatment is shown in Figure 33.

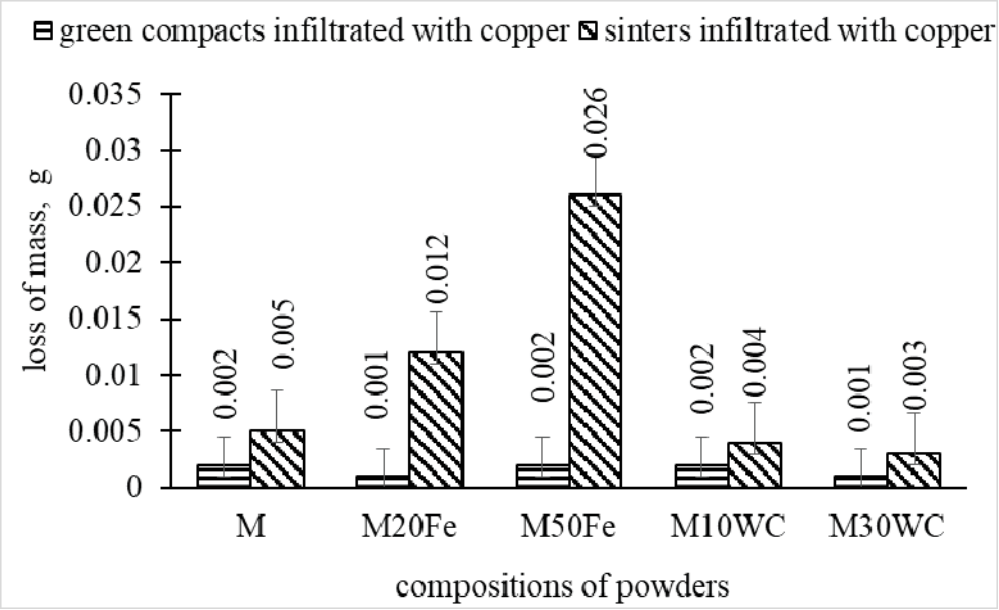

Fig. 32. Loss of mass of as infiltrated composites

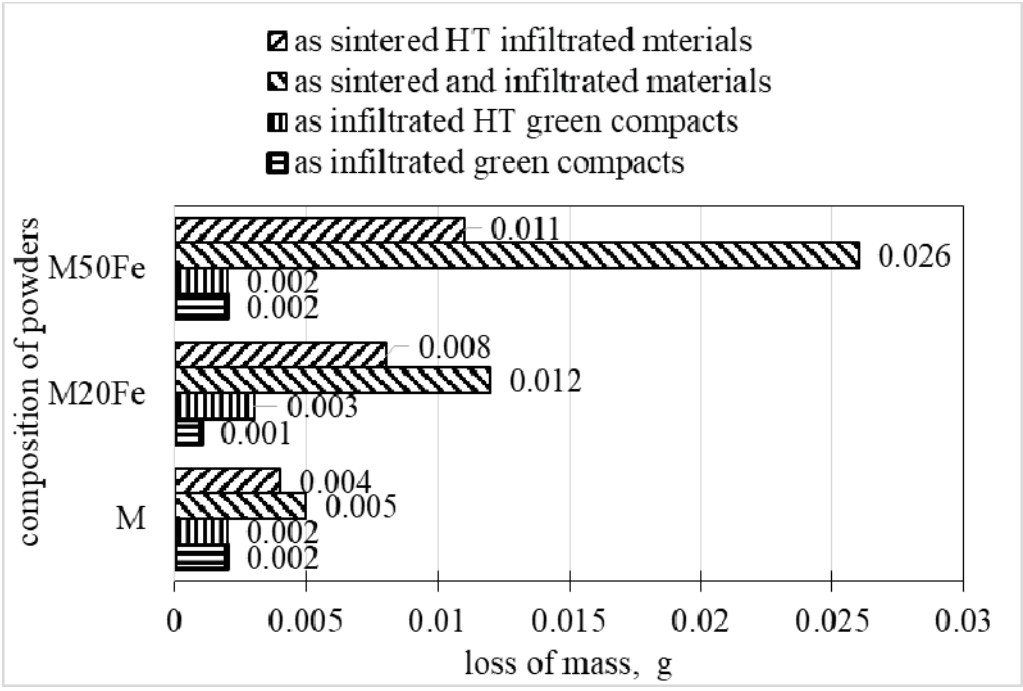

Fig. 33. Loss of mass of as infiltrated composites and after heat treatment (HT)

A summary of the tribological tests results presented in Figure 33 allows to conclude that heat treatment does not cause significant changes in wear resistance of materials obtained by direct infiltration of copper to green compacts. The situation is completely different when were considered materials after heat treatment produced direct infiltration of

as-sintered materials. In the case of materials with an iron addition, their abrasion resistance is increasing after heat treatment, which correlates with hardness measurements and observations of changes in the microstructure of these materials presented in section 3.3. The additional time of diffusion of alloying elements from steel to iron and the coffe effect observed close to Cu-iron boundary improve the iron particles properties, and it improves the tribological properties of the the whole material. It is equally important to determine the wear mechanisms of these materials. The sample surfaces obtained in the tribological contact were observed using a confocal type microscope. Characteristic surface topographies after the wear test are exemplified in Figures 34 and 35.

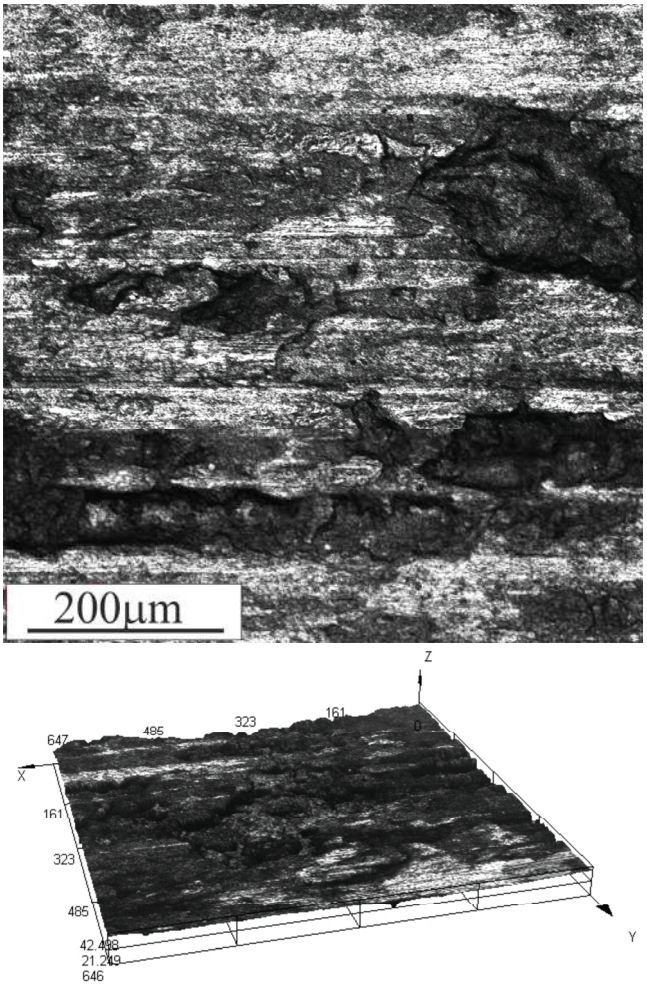

Fig. 34. Characteristic sample surface of the M after tribological tests

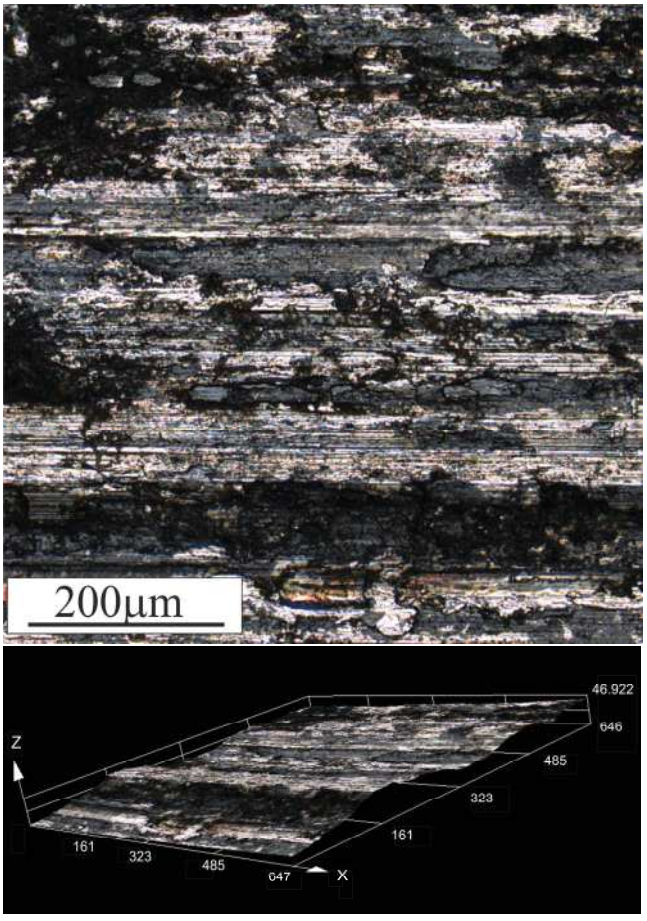

Fig. 35. Characteristic sample surface of the M50Fe materials after HT and after tribological tests

The surface topographies of M and M50Fe$_{HT}$ specimens indicate occurrence of different wear mechanisms (Figs. 34, 35). The carbides seen on the wear-surfaces are being crushed and pulled out of the composites microstructure to act as abrasive particles which increase the coefficient of friction but from Figure 34 it is also evident that there are ploughing and sideways displacement of material in M – probably in copper regions. Figure 35 shows smearing of iron over the surface of the as-infiltrated M50Fe$_{HT}$ as-infiltrated materials which implies marked contribution of adhesive wear, whereas excessive formation of iron oxides can cause the lowest coefficients of friction – but increases wear. Copper additions to these materials increase the contribution of micro-cutting and, presumably, adhesion wear which results in the highest friction coefficients.

4. Conclusions

Infiltration of porous skeleton made from HSS powder or HSS powder with additions of iron or WC with liquid copper has proved to be a suitable technique whereby almost fully dense materials are produced while maintaining low production costs. Direct infiltration of green compacts with copper results in the higher hardness and higher resistance to wear of the all kinds of examined materials, and allows to cut the production cost.

The mechanical properties of the examined composites depend on the iron content. The presence of iron decreases the hardness and increases the bending strength.

The mechanical properties of the HSSs based composites are strongly dependent on the tungsten carbide additions, the hardness increasing but decrease their bending strength with increasing the volume of WC.

The characteristic microstructure of composites based on high-speed steel and infiltrated with copper and with high-iron additions consists of HSSs matrix with MC, M_6C, ferrite, tempered martensite, residual austenite, and copper and iron areas. No precipitation of carbides in the iron area was observed, while on the iron copper boundary (in iron particles) the coffe effect was found. It consists in the precipitation of nanometric copper particles in iron during the tempering. This phenomenon combined with the diffusion of alloying elements from steel matrix to iron causes only a slight influence of the addition of iron Höganäs powders to high-speed steels. The source of alloying elements are M_6C type carbides located at the iron-HSS contact boundary, which dissolve during the sintering process at 1150°C.

The additions of WC to HSS powder result in some microstructural changes. There are typical microstructure of high speed steel composed of WC, MC, M_6C carbides type, ferrite, tempered martensite residual austenite and copper regions. The distribution of WC carbides depend on its contents and production process parameters. Tungsten-rich M_6C type carbide is formed during sintering as a result of the chemical reaction between the product of tungsten monocarbide dissolving and alloying elements from HSSs matrix. Studies have shown that the newly formed carbide at the grain boundary of HSS/WC additions differs in chemical composition from the typical M_6C carbide present in molybdenum type high speed steels. This new M_6C type carbide are strongly enriched in tungsten, and impoverished of iron, and molybdenum comparing to typical M_6C carbides. Stoichiometrically recognized carbide from XRD analysis is described by formula Fe_3W_3C-Fe_4W_2C, but after analyzing the chemical composition of the newly created carbide, it could be presented as $(Fe, Mo, Cr)_3(W)_3C$.

Acknowledgements

Research carried out as part of Research Subsidies, agreement No. 16.16.110.663.

References

[1] G. Greetham, Development and performance on infiltrated and non-infiltrated valve seat insert materials and their performance, Powder Metallurgy 3/2 (1990) 112-114.

[2] R.H. Plama, Tempering response of copper alloy-infiltrated T15 high-speed steel, The International Journal of Powder Metallurgy 37/5 (2001) 29-35.

[3] C.S. Wright, The production and application of PM high-speed steels, Powder Metallurgy 3 (1994) 937-944.

[4] L.A. Dobrzański, G. Matula, A. Várez, B. Levenfeld, J.M. Torralba, Structure and mechanical properties of HSS HS6-5-2- and HS 12-1-5-5-type steel produced by modified powder injection moulding process, Journal of Materials Processing Technology 157-158 (2004) 658-668, DOI: https://doi.org/10.1016/j.jmatprotec.2004.07.138.

[5] J.M. Torralba, G. Cambronero, J.M. Ruiz-Pietro, M.M. das Neves, Sinterability study of PM M2 and T15 HSS reinforced with tungsten and titanium carbides, Powder Metallurgy 36/1 (1993) 55-66, DOI: https://doi.org/10.1179/pom.1993.36.1.55.

[6] P.K. Samal, J.W. Newkirk (Eds.), ASM Handbook: Volume 7: Powder Metallurgy, ASM International, 2015, 1-907.

[7] M. Madej, J. Leżański, Copper infiltrated high speed steel based composites, Archives of Metallurgy and Materials 50/4 (2005) 871-877.

[8] M. Madej, J. Leżański, The structure and properties of copper infiltrated HSS based, Archives of Metallurgy and Materials 53/3 (2008) 839-845.

[9] M. Madej, The tribological properties of high speed steel based composites, Archives of Metallurgy and Materials 55/1 (2010) 61-68.

[10] L.A. Dobrzański, G. Matula, A. Várez, B. Levenfeld, J.M. Torralba, Fabrication methods and heat treatment conditions effect on tribological properties of high speed steels, Journal of Metarials Processing Technology 157-158 (2004) 324-330, DOI: https://doi.org/10.1016/j.jmatprotec.2004.09.051.
[11] L.A. Dobrzański, Goals and Contemporary Position of Powder Metallurgy in Products Manufacturing, in: L.A. Dobrzański (Ed.), Powder metallurgy – fundamentals and case studies, InTech, 2017, 1-16, DOI: http://dx.doi.org/10.5772/61469.
[12] E. Gordo, F. Velasco, N. Antón, J.M. Torralba, Wear mechanisms in high speed steel reinforced with (NbC)p and (TaC)p MMCs, Wear 239/2 (2000) 251-259, DOI: https://doi.org/10.1016/S0043-1648 (00)00329-X.
[13] L.A. Dobrzański, A. Kloc-Ptaszna, Fabrication, Structure, Properties and Application of Gradient Sintered Carbide-Steels with HS6-5-2 Matrix, in: L.A. Dobrzański (Ed.), Powder metallurgy – fundamentals and case studies, InTech, 2017, 199-222, DOI: http://dx.doi.org/10.5772/61469.
[14] F. Akhtar, Microstructure evolution and wear properties of in situ synthesized TiB_2 and TiC reinforced steel matrix composites, Journal of Alloys and Compounds 459/1-2 (2008) 491-497, DOI: https://doi.org/10.1016/j.jallcom.2007.05.018.
[15] G. Hoyle, High Speed Steels, Butterworth & Co. Publishers, Cambridge, 1998.
[16] S. Wei, J. Zhu, L. Xu, Effects of vanadium and carbon on microstructures and abrasive wear resistance of high speed steel, Tribology International 39/7 (2006) 641-648, DOI: https://doi.org/10.1016/j.triboint.2005. 04.035.
[17] Z. Zalisz, A. Watts, S.C. Mitchell, A.S. Wronski, Friction and wear of lubricated M3 Class 2 sintered high speed steelwith and without TiC and MnS additives, Wear 258/5-6 (2005) 701-711, DOI: https://doi.org/10.1016/j.wear.2004.09.069.
[18] W.C. Zapata, C.E. Da Costa, J.M. Torralba, Wear and thermal behaviour of M2 high-speed steel reinforced with NbC composite, Journal of Materials Science 33/12 (1998) 3219-3225, DOI: https://doi.org/ 10.1023/A:1004324729342.
[19] G.A. Baglyuk, L.A. Poznyak, The sintering of powder metallurgy high-speed steel with activating additions, Powder Metallurgy and Metal Ceramics 41/7-8 (2002) 366-368, DOI: 10.1023/A:1021113025628.
[20] W. Khraisat, L. Nyborg, P. Sotkovszki, Effect of silicon, vanadium and nickel on microstructure of liquid phase sintered M3/2 grade high speed steel, Powder Metallurgy 48/1 (2005) 33-38, DOI: https://doi.org/10.1179/003258905X37602.
[21] J.A. Jiménez, M. Carsı, G. Frommeyer, O.A. Ruano, Microstructural and mechanical characterisation of composite materials consisting of M3/2 high speed steel reinforced with niobium carbides, Powder Metallurgy 48/4 (2005) 371-376, DOI: https://doi.org/ 10.1179/174329005X79832.
[22] J.D. Bolton, A.J. Gant, Phase reactions and chemical stability of ceramic carbide and solid lubricant particulate additions within sintered high speed steel matrix, Powder Metallurgy 36/4 (1993) 267-274, DOI: 10.1179/pom.1993.36.4.267.
[23] J.D. Bolton, A.J. Gant, Heat treatment response of sintered M3/2 high speed steel composites containing additions of manganese sulphide, niobium carbide, and titanium carbide, Powder Metallurgy 39/1 (1996) 27-35, DOI: 10.1179/pom.1996.39.1.27.
[24] H.G. Rutz, F.G. Hanejko, High density processing of high performance ferrous materials, Proceedings of the International Conference & Exhibition on Powder Metallurgy & Particulate Materials, Toronto, Canada, 1994.
[25] L.A. Dobrzański, Engineering materials and materials design; Fundamentals of materials science and physical metallurgy, WNT, Warsaw, 2006, 1-1600 (in Polish).
[26] M. Madej, Copper infiltrated high speed steel based composites with iron additions, Archives of Metallurgy and Materials 54/4 (2009) 1083-1091.
[27] M. Madej, The tribological properties of high speed steel based composites, Archives of Metallurgy and Materials 55/1 (2010) 61-68.
[28] M.M. Oliveira, High-speed steels and high-speed steels based composites, International Journal of Materials and Product Technology 15/3-5 (2000) 231-251, DOI: 10.1504/IJMPT.2000. 001251.
[29] M. Madej (inventor), Method for heat treatment of infiltrated composites on HSS, AGH University of Science and Technology, Int.Cl.: C22C 33/02; Patent description; PL 219902 B1; Granted 2014-10-24; Published: 2015-07-31, Notification no: P.397461 from 2011-12-19 (in Polish).
[30] M.M. Serna, E.R.B. Jesus, E. Galego, L.G. Martinez, H.P.S. Corrêa, J.L. Rossi, An Overview of the

Microstructures Present in High-Speed Steel – Carbides Crystallography, Materials Science Forum 530-531 (2006) 48-52, DOI: https://doi.org/10.4028/www.scientific.net/MSF.530-531.48.

[31] J. Richter, J. Szala, J. Cwajna, Selective Evaluation of Carbide Phase in Economical High-Speed Steel of Elevated Hardness, Proceedings of the 6th International Conference Stereology and Image Analysis in Materials Science "STERMAT 2000", Cracow, 2000, 337-342.

[32] J. Richter, J. Szala, J. Cwajna, Quantitative Assessment of PVD Layers Deposited on Commercial and Economical High-Speed Steels, Proceedings of Sixth International Conference Stereology and Image Analysis in Materials Science "STERMAT 2000", Cracow, 2000, 343-350.